

CHAPTER 1: INTRODUCTION

1.1 Introduction of Schiff base.

The Schiff base is named after a German chemist called Hugo Schiff, who is responsible for discovering the compound in 1864 (Tidwell et al., 2008). The compound is formed via condensation reaction of a primary amine with an aldehyde or a ketone under specific condition. It is rapidly becoming an important class of compounds in medicinal and pharmaceutical areas as the ease of C=N formation, the synthetic flexibility of the ligands, the sensitivity towards the central metal ion, and the structural resemblance with natural biological substances, has brought considerable interest to this field (Nishat et al., 2010).

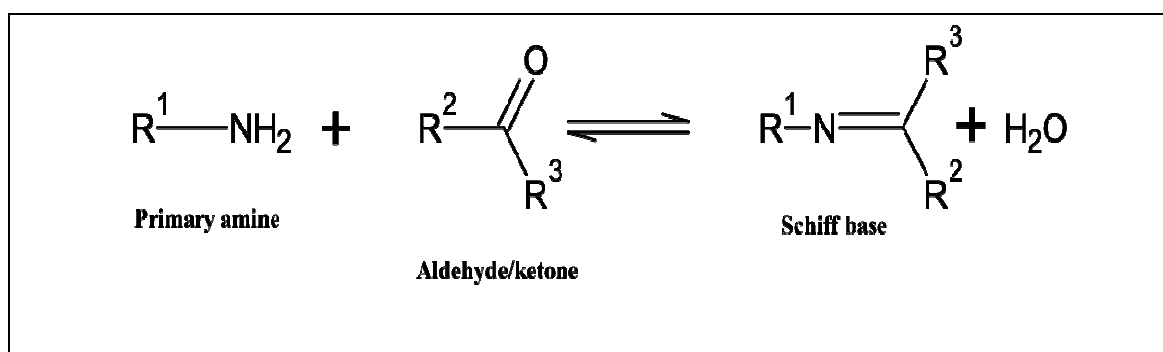


Figure 1.1: Formation of Schiff base

1.2 The Chemistry of Schiff base

Schiff base, commonly applies straight forward reaction pathways. The process conveniently occurs in mild conditions, without catalyst and sometimes with the application of heat. The double bond of the carbonyl functional group in aldehyde or ketone is strongly polarized by electronegative oxygen atom. The nucleophilic attack which occurs at the carbon needs very little energy to distort the polarized p-bond so that oxygen becomes negatively charged. On the other hand, the difference in electronegativity of carbon and nitrogen in C=N is less than electronegativity difference of C=O causing the imine group to be less polar. When the nucleophilic attack occurs at

the carbon of the imine, an unstable intermediate with negative charge on nitrogen will be generated. Consequently, imine is less reactive to nucleophilic attack compared to carbonyl group.

The nucleophilic amine will react with aldehyde or ketone to form an unstable carbinolamine or hemiaminal, with both the amino and hydroxyl functional group attached to the same carbon and followed by the elimination of water molecule. Since the carbinolamine is an alcohol, it undergoes acid-catalyzed dehydration but the amines are basic compounds, thus the acid concentration cannot be too high. Excess acidity will cause the amine to protonate and become non-nucleophilic and affects carbinolamine formation, as the equilibrium will be pulled to the left. Therefore, Schiff base reaction favours mild acidic condition.

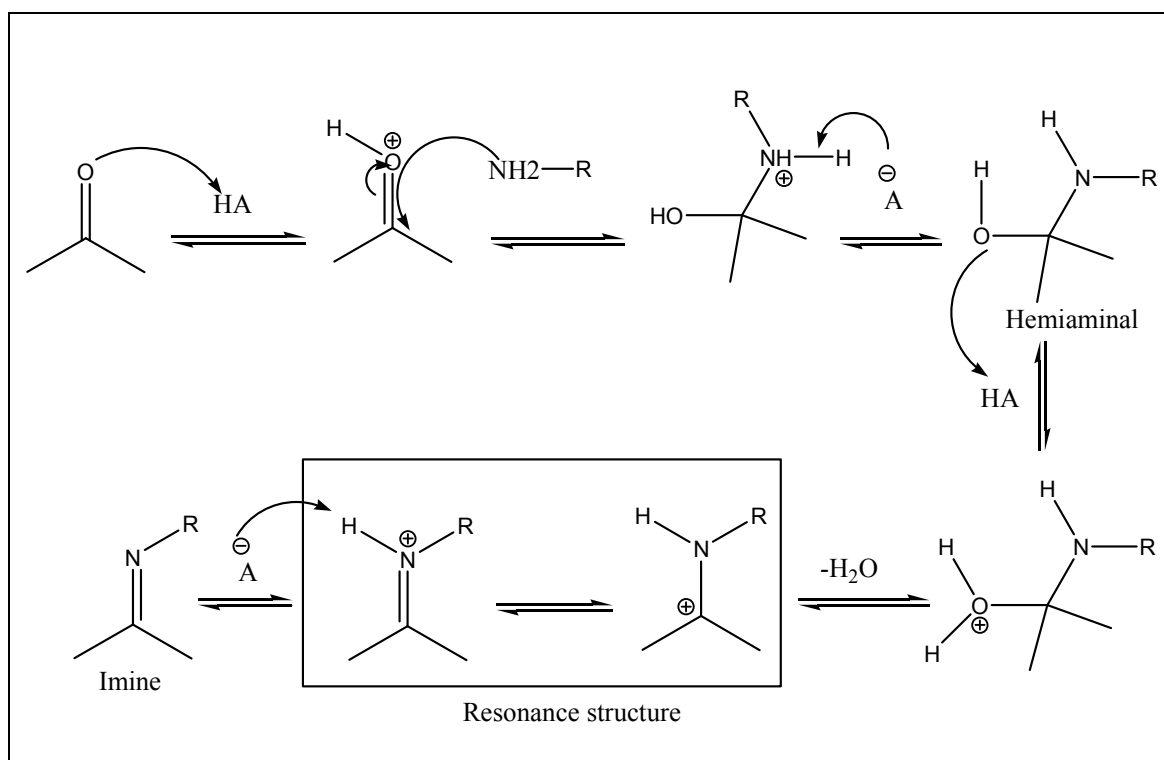


Figure 1.2: Schiff base formation in acidic environment

Schiff bases of aryl moiety are relatively more stable than that of alkyl substituent. The presence of aryl substituent with effective conjugation will substantially stabilize the

Schiff base compound (Hine et al., 1967, Campbell et al., 1944). Aliphatic Schiff base compounds on the other hand, are readily polymerized and unstable (Brewster, 1924).

The chemistry of Schiff base metal complexes has been given considerable attention for the previous two decades, attributed to their stability and biologically active properties (Liu et al., 1996). Some drugs show higher activity when administered as metal complexes rather than free ligands (Ramesh et al., 2003).

The synthesis applied by Schiff during his extensive study involved the reaction under azeotropic distillation (Moffet, 1963), before molecular sieves was introduced to remove water from the system completely (Taguchi et al., 1971). In situ method on the other hand, came into practice after 1990, using dehydrating solvents such as tetramethyl orthosilicate or trimethyl orthoformate (Love et al., 1993, Look et al., 1995). However, this method is only suitable for reactions of carbonyl compounds with high electrophilicity and strong nucleophilic amines (Chakraborti et al., 2004). Chakraborti suggested the use of Bronsted-Lowry or Lewis acids as an alternative to activate the carbonyl group of aldehydes catalyze the nucleophilic attack by amines, and to dehydrate the system as the final step (Chakraborti et al., 2004).

1.3 Cancer

In the year 2000, 10 million people were diagnosed with cancer, leading to 6.2 million deaths, an increase of about 22% since 1990 (World Health Organization, WHO). At least one in three people develop cancer, one in four men and one in five women die from it although improvements in public health and medical care towards the risk of cancer has increased dramatically in recent years. WHO has predicted that the number of new cases will increase by 5 to 15 million each year by 2020. For this reason, cancer

prevention and control has become a major health issue. The most common type of cancer is lung cancer followed by breast cancer and colon-rectum cancer.

Cancer is defined as a disorder of cells that appears as a tumor made up of a mass of cells. Tumors are usually recognized by the fact that the cells have shown abnormal proliferation and differ from normal cells in the lack of respond to normal control mechanisms. Generally, tumors are categorized into three key groups. Benign tumors which grow locally causing damage by local pressure or obstruction but do not spread to distant organs. Another type of tumor namely in situ tumors commonly develops in the epithelium, sharing the similar morphological appearance of cancer cells but remains in the epithelial layer. On the other hand, malignant tumors are fully developed with a specific capacity to invade and destroy normal cells. The tumor cells produce a range of protein which stimulates the growth of blood vessels into the tumors. The fragments of the tumors may be carried in these vessels to local lymph nodes or to distant organs where secondary tumors may be produced. This spreading is the main problem in providing the treatment compared to localized tumors that can be easily removed by surgical procedure (or surgery) or radiation.

The major and specific causes for some cancers are known to be smoking for lung cancer, reproductive and hormonal factors for breast cancer and human papillomavirus (HPV) infection that leads to cervical cancer. Other related factors responsible for the disease include diet-related factors, radiation exposure, genetic predisposition and environmental pollutions (Franks, 2005).

1.3.1 Anticancer drugs

The exploitation of unique properties of metal ions led to the landmark discovery of the Cisplatin (Jung et al., 2007), although the application is severely limited by its own toxic side-effects such as neuro-, hepato- and nephrotoxicity (Bruijnininx et al., 2008,

Jung et al., 2007). The effort to develop new anticancer drugs back then was according to the cisplatin paradigm, in which the anticancer agents target DNA directly to generate lesions which trigger cell death. Platinum–DNA adducts, which are formed following the uptake of the drug into the nucleus of cells, activate several cellular processes that mediate the cytotoxicity of these platinum drugs (Wang et al., 2005). Therefore, the challenge is raised on the designing of drug delivery systems capable of delivering the agent to tumour cells only. One of the strategies is by encapsulating the cisplatin and carboplatin in the hollow protein cage of the iron storage protein ferritin, which can be internalized by some of tumour tissues. The application of such method allows the potential of cytotoxicity against the rat pheochromocytoma cell line (PC12) (Yang et al., 2007). Human thioredoxin reductase (hTrxR) is an interesting target for anticancer drugs due to its association with many cellular processes such as antioxidant defense, redox homeostasis and apoptosis regulator protein p53 making it strongly linked with tumor proliferation (Urig et al., 2006a). Gold(I) complexes are found to be among the most potent inhibitors of hTrxR, due to its high electrophilicity and its preference for the selenocysteine residue of hTrxR. Phosphole–gold(I) complexes are found to be highly potent, nanomolar inhibitors of hTrxR and the related human glutathione reductase (hGR) (Urig et al., 2006b). Gold(III) complexes of thiocarbamates for instance showed higher cytotoxicity *in vitro* than cisplatin. It inhibits the tumour cells at proteasome which results in induction of apoptosis (Milacic et al., 2006).

1.4 Antioxidant

When metabolism reactions take place in our body, cells naturally produce free radicals as by-products. During exchange reaction, electrons will be transferred from the atom of one molecule to another molecule by oxidation and reduction process. Stable atom has an even number of electron in the outer orbital. During oxidation, an electron loss leaves

an odd number of unpaired electrons producing a highly unstable free radical. The free radical is known to be responsible to the oxidative damage of DNA that causes improper reproduction of cells leading to health problems like cancer, heart disease, premature aging and diabetes (Sen et al., 2000).

Majority of complex living things require oxygen for their existence. However, the production of reactive oxygen species (ROS) along the metabolic pathways will cause damage mainly by chemical chain reactions or by oxidizing DNA or protein. The disturbance caused by these ROS to the redox status of the body is reduced by two major classes of endogenous protective mechanisms (i.e. enzymatic or non-enzymatic) Both enzymatic and non-enzymatic oxidants work as a complete unit to detoxify the ROS in intracellular and intercellular environments. In general, antioxidants act as “free radical scavengers” that could contribute an electron to a damaging free radical, and subsequently convert it to a harmless molecule. These scavengers are strategically distributed throughout the body cell to allow maximum intracellular protection.

Primary antioxidant enzymes include superoxide dismutase (SOD), glutathione peroxidase (GPX), and catalase (CAT) which detoxifies a particular ROS. Non-enzymatic antioxidants comprise of glutathione, vitamin E, vitamin C, lipoic acid, bilirubin and ubiquinone (Sen et al., 2000).

This thesis contains 4 chapters. Chapter 2 presents the literature survey on the related topic of the study including the biological importances of salicylaldehyde and hydroxyacetophenone benzohydrazone compounds and their metal complexes. Chapter 3 contains experimental methods and elucidation techniques applied to characterize the compounds. This chapter also includes the procedures for the cytotoxicity and antioxidant activities evaluation. Chapter 4 discusses the findings of the study. A list of references and appendices are included at the end of the thesis.

CHAPTER 2: LITERATURE REVIEW

2.1 The Schiff bases.

Inspired by the effort of Jorgensen and Werner in coordination chemistry, Ettlign isolated the first Schiff base metal complex from the reaction of cupric acetate, salicylaldehyde and aqueous ammonia (Ettlign, 1840). It was followed by a remarkable discovery of an important synthetic technique of preparing salicylaldehyde complex by reacting the pre-formed metal-salicylaldehyde compound with primary amine (Schiff, 1869). The systematic studies of Schiff base complexes were later commenced by Pfeiffer and his co-worker (Pfeiffer et al., 1936).

Studies have been done vastly to reveal the chemistry and the versatility of the applications of Schiff base and its metal complexes. Schiff base hydrazones of pyridoxal phosphate, and its analog, for instance, has been investigated systematically in order to have better understanding of the reaction mechanism of vitamin B6-containing enzyme (Maghler et al., 1982). Nishinaga and his co-worker reported a unique mechanism for a cobalt-Schiff base complex-catalyzed monooxygenation of alkenes. The complexes were found to efficiently catalyze the oxygenation of alkenes substituted with an aromatic or an electron-withdrawing group without carbon-carbon bond cleavage (Nishinaga et al., 1988). Amine terminated liquid natural rubber (ATNR) yielded from photochemical degradation of natural rubber, undergoes condensation process with glyoxal and produce Schiff bases with enhance aging resistance (George et. al., 1993).

Recently, Ray and her group studied cobalt(II) and copper(II) complexation of a tridentate NNO donor Schiff base ligand in presence of azide ions. The coordination under different synthetic conditions gives rise to unusual dinuclear and polynuclear species. One of the complexes demonstrated a very strong antiferromagnetic exchange interaction ($J = -252(1) \text{ cm}^{-1}$) through the single $\mu_{1,3}$ -azido bridge (Ray et al., 2011),

twice the highest value for a double μ 1,3-azido bridged copper (II)-dinuclear compound ($J = -105 \text{ cm}^{-1}$) (Sarkar et al., 2005).

Polymeric Schiff bases and their metal complexes have been found to play roles in pharmacological and non-pharmacological fields. The antimicrobial activity of the coordinated polymeric Schiff base showed significant enhancement due to the additional number of C=N bond and chelation. The presence of metal ions influenced the solubility, conductivity and dipole moments, thus improving the biological activity (Nishat et al., 2010). Other important applications of polymeric Schiff bases include as solar energy converter (Grayson et al., 1983), and removal of SO_x and NO_x from the environment (Toshima, 1991). Ironically, aromatic Schiff bases and their metal complexes also took part in the polymerization reaction as catalysts (Kudryavstev et al., 1962).

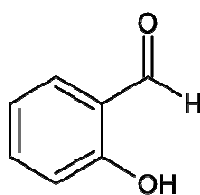
Quite a number of research have been done on the chemistry and the biocidal activities of transition metal complexes containing O,N and S,N donor atoms due to their structural lability and sensitivity to molecular environment (Chakraborty et al., 1996). The important factors such as coordination geometry, number of coordinated ligands and the donor group are the key factors for metalloproteins to carry out specific physiological functions (Klement et al., 1999).

The biological role plays by metals and chelation have been intensively studied (William, 1972, Crim et al., 1967, Chakraborty et al., 1996) and established the fact that the chelated metal complexes exhibit higher antitumor activity compared to their organic moiety. Chelation is reported as the cause and cure for many diseases as it changes the biological properties of the ligands and metal moiety drastically (Drabent et al., 2004).

2.2 The Importance of benzohydrazone-related compounds

Nakanishi in his studies had used di-2-pyridyl ketone benzohydrazone (DPKBH) to determine the trace amount of iron(II) spectrophotometrically, in connection with the extraction process. The green iron(II) complex is quantitatively extracted into benzene. The proposed method showed relative selectivity for iron(II) and is applied to the determination of total iron in natural waters (Nakanishi et al., 1986). In the same year, Garcia-Vargas and his co-worker begin the studies of coordination of 1,2-cyclohexanedione bis-benzohydrazone with titanium(IV). This simple yet selective method was later applied commercially to determine titanium in bauxite, Portland cement, amphibolites and granites (Garcia-Vargas et al., 1986).

2.3 Salicylaldehyde



(1)

Salicylaldehyde ($C_6H_4CHO-2-OH$) (1) is one of three isomers of hydroxybenzaldehyde and it can be prepared via Reimer-Tiemann reaction by heating sodium phenolate and chloroform with sodium hydroxide. It is a clear, colourless oily liquid and has a bitter almond odor and burning taste at higher concentration. At a lower concentration, it smells like buckwheat. Over the years, study involving salicylaldehyde has been done tremendously by researchers all over the world for its advantage as a key precursor to a variety of chelating agents, some of which are commercially and biologically important. In Dakin reaction, salicylaldehyde undergoes oxidation with hydrogen peroxide to yield catechol (Dakin, 1941). Salicylaldehyde also involves as product and reactant in enzymatic degradation of naphthalene (Caspi et al., 2010).

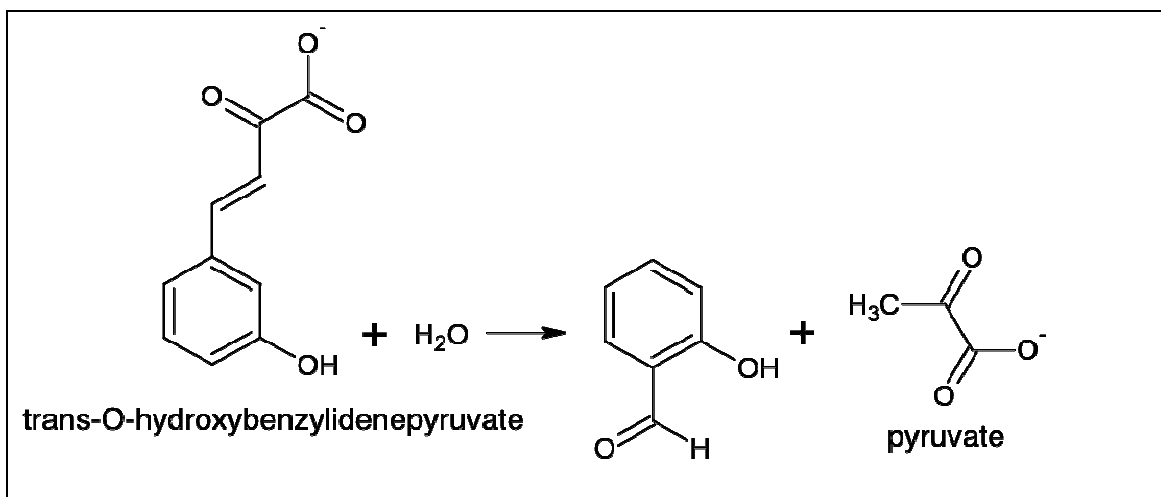


Figure 2.1: Salicylaldehyde as a product

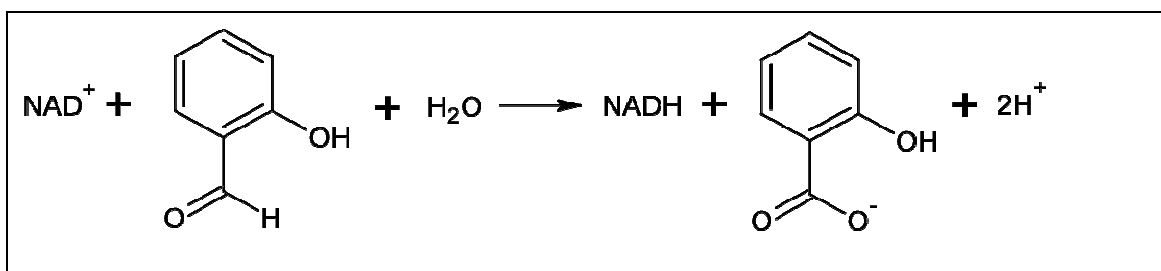
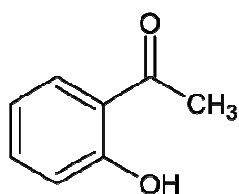


Figure 2.2: Salicylaldehyde as a reactant

2.4 Acetophenone



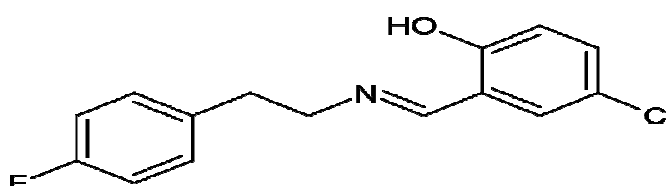
(2)

Acetophenone (2) is the simplest form of aromatic ketone, commercially obtained from benzene with acetic anhydride or acetic chloride by Friedel-Craft reaction or by air oxidation of ethylbenzene, as a by-product of cumene or acrylonitrile. Acetophenone and its derivatives, substituted with various functional groups are ingredients of flavor & fragrance for soaps, detergents, cosmetics, and perfumes as well as in foods, beverages, and tobacco. Specifically, hydroxyl substituted acetophenone or namely

hydroxyacetophenone is used as building blocks for the synthesis of rubbers, plastics, pharmaceuticals, agrochemicals and flavor and fragrances.

2.5 Biological Importance of salicylaldehyde and acetophenone

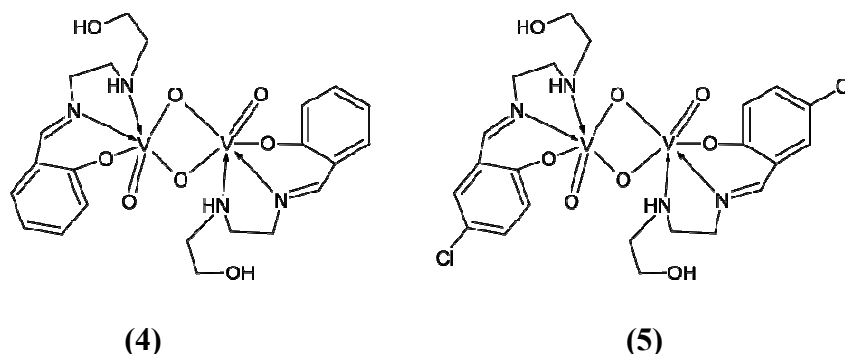
Felton reported that the presence of halogen atom in the aromatic ring of salicylaldehyde is the key factor of salicylaldehyde-contained Schiff bases to have better antibacterial and antifungal activities (Felton et al., 1947). Applying the same conception, Lei Shi and his team reacted 26 different types of primary amines with 5-chlorosalicylaldehyde. The antibacterial and antifungal activities of the compounds synthesized were screened. Among all the compounds tested, the most favorable antimicrobial activity was shown by (E)-4-chloro-2-((4-fluorobenzylimino)-methyl)phenol (**3**) (Shi et al., 2007). Schiff base complexes derived from amine and 4-hydroxysalicylaldehyde was also found to exhibit promising anticancer activity against Ehrlich ascites carcinoma (EAC) (Zishen et al., 1993). It is believed that the higher the hydrophilicity and the aromaticity of the compounds, the higher the activity of the compounds (Shi et al., 2007).



(3)

Recently, a comparative study on dinuclear vanadium(V) complexes derived from salicylaldehyde (**4**) and 5-chlorosalicylaldehyde (**5**) was done. At the doses of 10.0 and 20.0 mg V kg⁻¹ complex (**5**) showed a significant decrease in the blood glucose level as the result of in-vivo test for hypoglycemic activity. The complex is believed to have an antidiabetic potency due to its blood glucose-lowering activity and the ability to

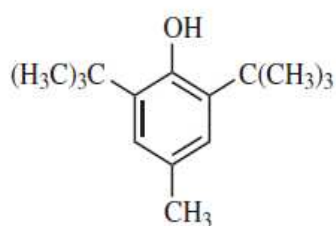
improve glucose tolerance. However, complex **(4)** did not show blood glucose-lowering effect (Xie et al., 2010).



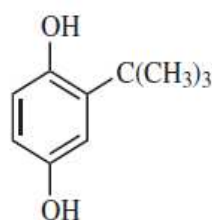
2.6 The biological importance of Polyhydroxy Benzohydrazone.

Many investigations were carried out on the polyhydroxyl benzohydrazone compounds which are believed to possess health benefits by quenching free radicals, regulate nitric oxide, decrease leukocyte immobilization, induce apoptosis, inhibit cell proliferation and exhibit phytoestrogenic activities that may contribute to their protective role in cancer and cardiovascular diseases (Hingdon et al., 2003, Yang et al., 2001).

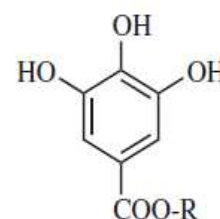
Various disorders such as cancer, diabetes, and cardiovascular related diseases have been associated with the generation of reactive oxygen species (ROS) (Ratnam et al., 2006). The major antioxidants currently used in foods are monohydroxyl or polyhydroxyl-phenol compounds with various ring substitutions.



Butylated hydroxytoluene (BHT)



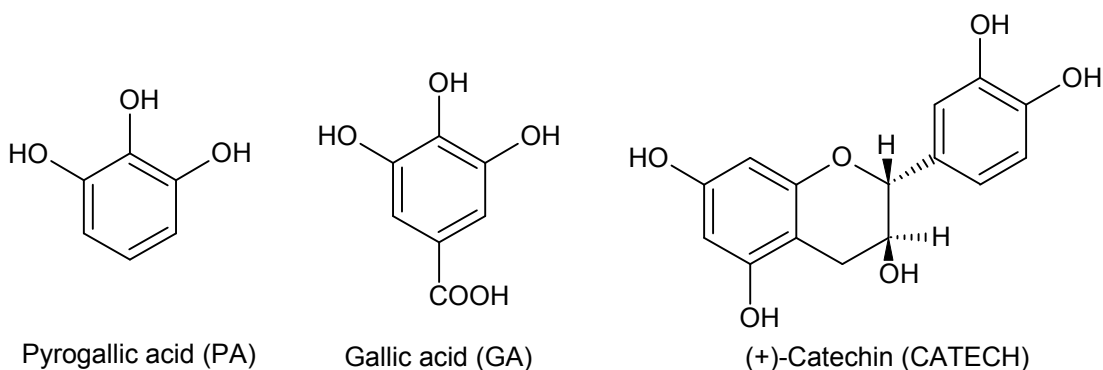
Tertiary-butylhydroquinone (TBHQ)



Gallates

The acidity of the compounds due to the low activation energy of the hydrogen donation is believed to play a major role on the ability of these compounds to quench the free radicals (Rice-Evans et al., 1999). It is also caused by the delocalization of the π -electron of the benzene ring while remaining relatively stable. One of the most

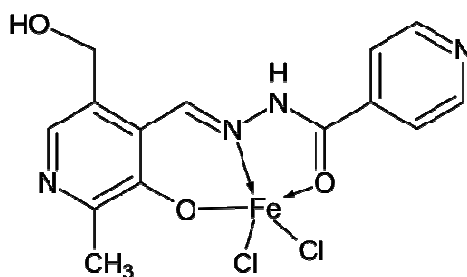
important classes of organic polyphenol is gallic acid (GA) and its derivatives, which are found naturally in many phytomedicine. The studies on this compound have shown significant biological activities such as antitumor (Zhang et al., 2008), neuroprotective, and antioxidant (Arunkumar et al., 2006).



2.7 The biological importance of Salicylaldehyde Benzohydrazone and Hydroxylacetophenone Benzohydrazone.

Chelating agents are noted as removers of toxic metal ions accumulated in the body (Chenoweth, 1967). Patients diagnosed with β -thalassemia rely on treatment with iron chelating drugs throughout their lifetime. Back in 1982, the only available agent desferrioxamine B was known to be unsatisfactory due to its chronic toxicity, efficacy and inconvenience of administration thus, the challenge has arisen to search for better drugs. (Waxman et al., 1982)

T. B. Murphy studied the coordination chemistry of the interaction between iron(III) and the most promising chelating agent called isonicotinoyl hydrazone of pyridoxal (PIH) (**6**) that was found to have the ability to induce substantial iron excretion in rats (Murphy et al., 1982a). As the coordination occurs, the ligand remained in the natural form as the protons are transferred from phenolic oxygen atom and the hydrazidic nitrogen atom to pyridine nitrogen atoms (Thompson et al., 1980).

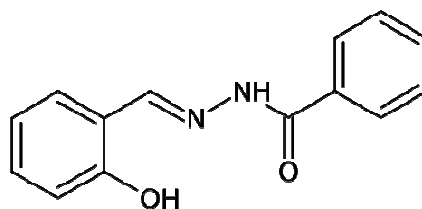


(6)

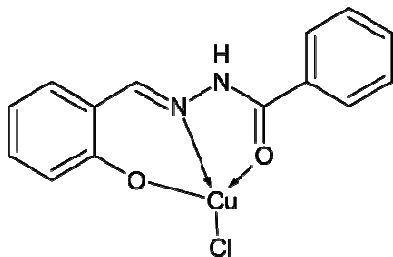
The observations when the rats are administered with PIH are consistent with the iron-PIH complex in-vivo. The bile flow contains iron in concentrations up to 80mg/ml and becomes deep red-brown in colour (Pippard et al., 1981).

The group also studied the inhibition of DNA synthesis in cultured rodent and human cells. A series of tridentate agents of pyridoxal and salicylaldehyde was synthesized and significant inhibitory activity was exhibited by copper(II) complex of salicyl benzohydrazone (SBH) (7) (Johnson et al, 1982). Both the ligand and copper complex was found to be non-toxic to mice and responded positively to different cell types. The capability of the ligand to chelate the iron established the idea that it was also capable of binding with essential metal ion in membrane cell in competition with endogenous ligand (Johnson et al., 1982).

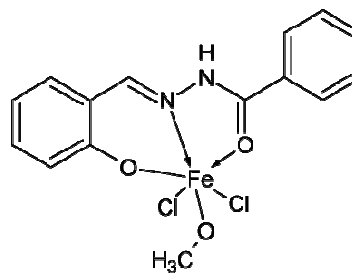
Single crystals of copper(II) (8), and iron(II) (9) complex of salicyl benzohydrazone (SBH) was obtained and the x-ray diffraction analysis was later published (Aruffo et al., 1982). In coordination to copper(II) and iron(II) ion, SBH remains as planar, neutral and binds via three terminals, phenolic and amide oxygens and azomethine nitrogen. The iron complex is 6-coordinate while the copper complex bears square planar 4-coordinate geometry. This is ironic with a proposal made by Iskander et al in his paper stating that the complex is 5-coordinate based on infrared evidence (Iskander et al., 1975).



(7)



(8)



(9)

M. Mohan and his research colleague studied the antitumor activity of the iron complexes of 3- and 5- substituted salicylaldehyde against P338 lymphocytic leukemia in mice. However, all the complexes were not bioactive at the tested dosage (Mohan et al., 1987).

In 1994, Ainscough and his co-worker introduced the antitumor study of copper salicyl benzohydrazone complexes with hexafluorosilicate coordination via in-situ reaction of fluoride on silica. The structure modification yielded a discrete centrosymmetric dimer and the ligands bridged by SiF_6^{2-} anion. With three donor atoms from the monoionic ligand, Si bridge via fluorine atom, and oxygen from a water molecule, the dimer employed distorted square pyramidal. Physicochemical studies revealed that the involvement of hexafluorosilicate anion enhances the stability and the packing of the complex in solid state due to the overlapping of π electron density in the delocalized ligand system (Ainscough et al., 1995).

In an article published later, they reported that by changing the reaction condition, the formulation of the complexes and the hydration number will be varied. In a very acidic condition, a complex of natural ligand isolated while in a weakly or neutral media,

monoanionic ligand was obtained. In the presence of a base, only highly insoluble dianionic complex was separated (Ainscough et al., 1998)

On the other hand, hydroxyacetophenone benzohydrazones and their transition metal complexes showed significant anti-fungal activity against *Rizoctonia* sp. and *Stemphylium* sp. but moderate antibacterial activity against *Clostridium* sp. and *Pseudomonas* sp. At higher concentrations of the compound, the activity is apparently increased (Singh et al., 2008, Singh et al., 2001).

Octahedral complexes derived from chelation of salicyl benzohydrazones and hydroxyacetophenone benzohydrazones with ruthenium metal, exhibit a higher activity compared to respective ligands against the same microorganism under identical conditions of experiment (Jayabalakrishnan et al, 2003). The formation of hydrogen bonding between the azomethine group (-C=N-) and microbes or ribosomes of microbial cells are believed to be responsible to the normal cells interference (Karvembu et al., 2001).

2.8 The objective of Study

The primary objectives of this study are:

1. To synthesize two series of benzohydrazone Schiff bases derived from substituted salicylaldehyde and hydroxyacetophenone.
2. To coordinate the prepared Schiff base ligands with zinc(II) and copper(II) metal ions.
3. To characterize the compounds by means of IR, ^1H NMR, ^{13}C NMR, UV-visible, CHN, X-ray crystallography, and metal composition analysis by atomic absorption spectroscopy (AAS)

4. To evaluate the cytotoxicity and anti-oxidant activities of the prepared ligands and their metal complexes.

CHAPTER 3: RESEARCH METHODOLOGY

3.1 Reagents and Solvents

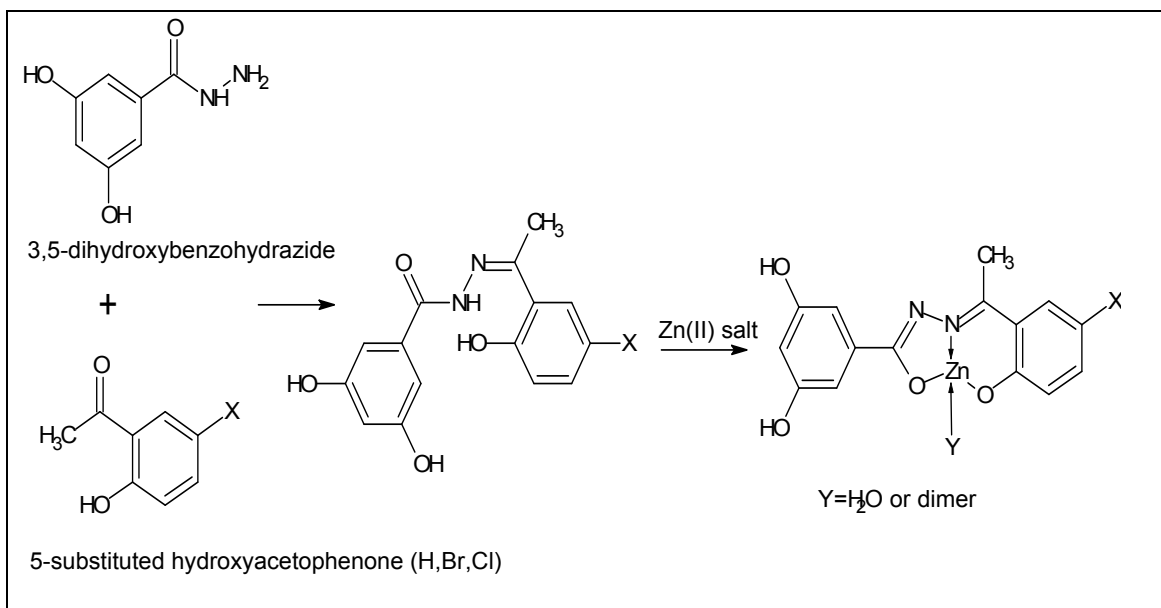
Methyl 3,5-dihydroxybenzoate, 2-Hydroxyacetophenone, 5-Bromo-2-hydroxyacetophenone, 5-Chloro-2-hydroxyacetophenone, 5-Chlorosalicylaldehyde (SIGMA ALDRICH), Salicylaldehyde, 5-Bromosalicylaldehyde, hydrazine (MERCK), Copper(II) acetate, Copper(II) chloride, Zinc(II) acetate, Triethylamine, Ethanol, and Dimethyl sulphoxide were used without further purification.

3.2 Experimental Instrumentation

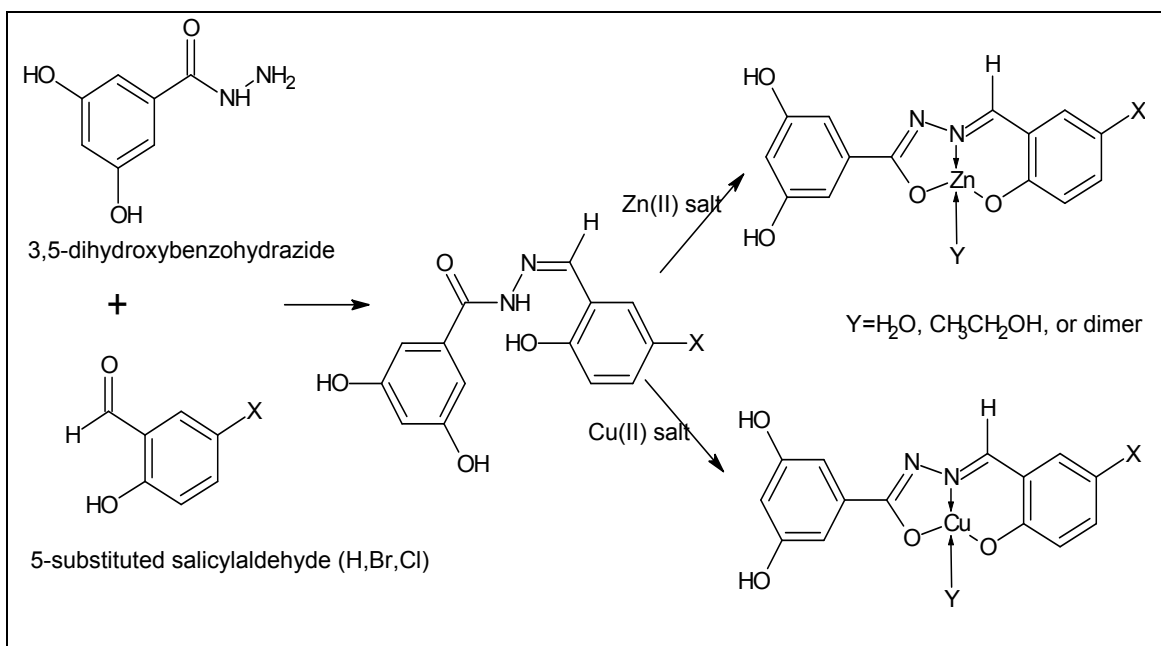
Infrared spectra of the compounds synthesized were recorded by Perkin-Elmer FTIR (Fourier Transform Infra-Red) spectrometer for frequencies 4000-400 cm^{-1} using KBr pellets. The ^1H and ^{13}C NMR was performed on Lambda JOEL 400MHz and ECA JOEL 400MHz FT-NMR with deuterated DMSO as solvent. The UV-visible spectra for solutions of the complexes were recorded with UV-1650PC Shimadzu UV-Vis spectrophotometer in the region of 300-800nm using DMSO as solvent with the concentration of the sample at $1 \times 10^{-6}\text{M}$ and metal composition analysis by atomic absorption spectroscopy(AAS) was performed using Perkin Elmer AAAnalyst 400. Elemental analysis for determination of C, H, N composition were performed by using Perkin Elmer 2400 Series II CHNS/O Analyzer. The single crystal X-ray diffraction data collection of some ligands was performed on Bruker Apex II CCD diffractometer at 100K employing graphite-monochromated Mo $K\alpha$ radiation ($\lambda=0.71073\text{\AA}$). The intensities were collected using the $\omega - 2\theta$ scan mode in the range of $3.1^\circ < \theta < 26.0^\circ$. All structures were solved using direct method by SHELXS-97 program (Sheldrick, 2008) and refined by full matrix least-square method on F^2 using SHELXL-97 program package (semi-empirical absorption corrections were applied using SADABS program).

3.3 General preparation of ligands and their metal complexes.

BzyHAP Series

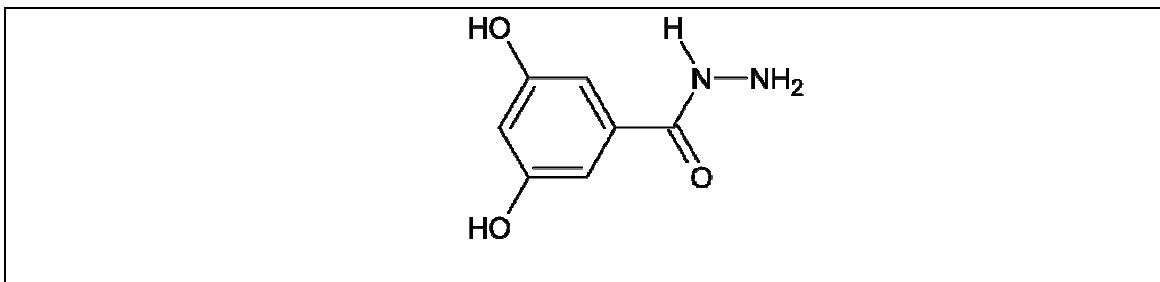


BzySAL Series



3.4 Preparation of starting material

3.4.1 3, 5-dihydroxybenzohydrazide

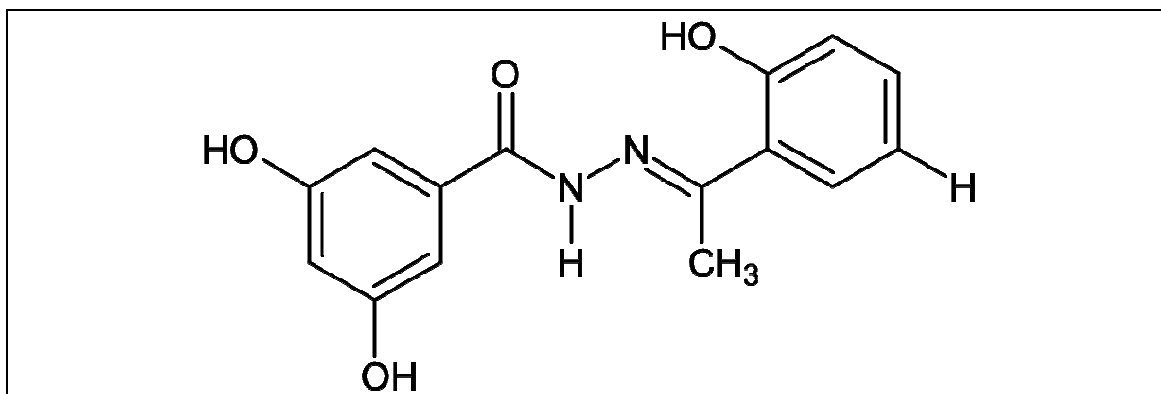


The mixture of Ethyl 3, 5-dihydroxybenzoate (5.0g, 30.0mmol) and excess of hydrazine hydrate was first stirred at room temperature for about an hour before 40ml ethanol was added to the mixture. The reaction was then refluxed for another 12 hours and gave a brown solution. Crystals of 3, 5-dihydroxybenzohydrazide were deposited over a period of few days. The solid was then filtered, washed with water, and air-dried (54% yield). IR($\nu_{\max}\text{cm}^{-1}$): 1659 (C=O), 3282 (N-H); ¹H NMR (ppm, 400 MHz, DMSO) δ_{H} : 9.5 (1H, s, H-N), 9.3 (2H, s, H-O_{Bzh}), 6.6-6.3 (3H, m, H-Ar). 4.4 (2H, s, H₂-N), CHN (% found (% calculated)): C 49.9 (50.0), H 4.3 (4.8), N 16.9 (16.7).

3.5 Series 1: Hydroxyacetophenone Benzohydrazone

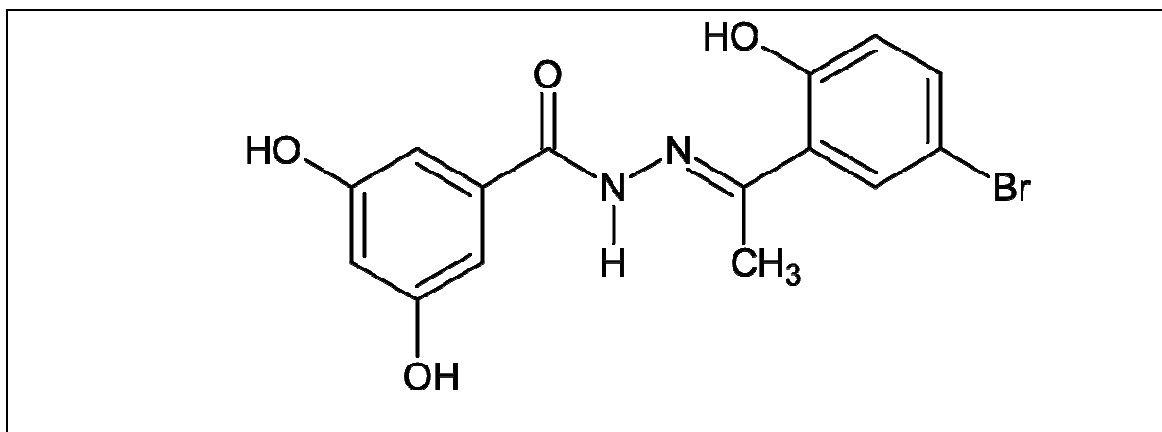
Preparation of the ligands

3.5.1 (BzyHAP-H)



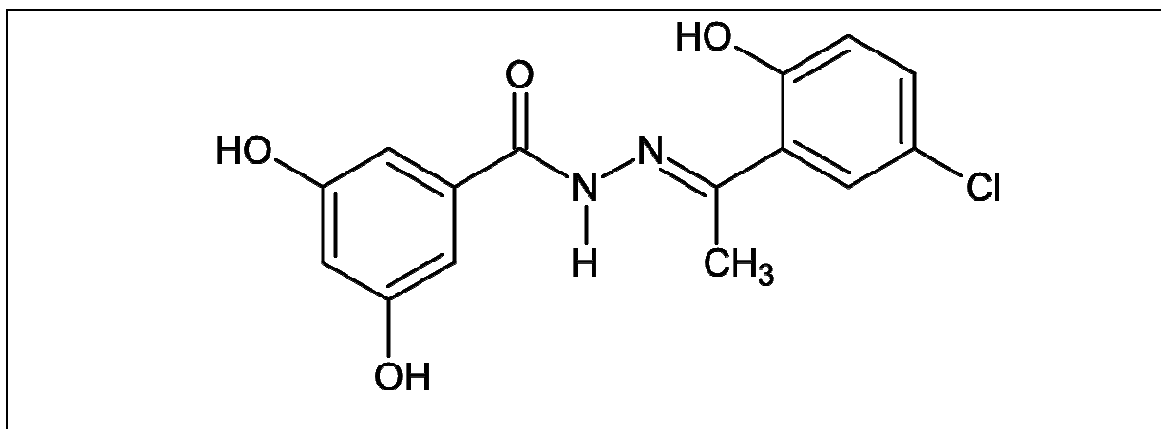
To a solution of 3, 5-dihydroxybenzohydrazide (0.8g, 5.0mmol) in 30ml of ethanol, 2-hydroxyacetophenone (0.6ml, 5.0mmol) was added drop wise and the reaction mixture was refluxed for 2 hours. A pale brown precipitate formed was filtered, washed with ethanol, and dried. (41% yield); IR(ν_{\max} cm⁻¹): 1642 (C=O), 1611 (C=N), 1003 (N-N), 3314 (O-H), broad (N-H); ¹H NMR (ppm, 400 MHz, DMSO) δ_{H} : 13.4 (1H, s, H-N), 11.3 (1H, s, H-O_{HAP}), 9.7 (2H, s, H-O_{Bzh}), 7.6-6.4 (7H, m, H-Ar), 2.4 (3H, s, CH₃); ¹³C NMR (ppm, 100 MHz, DMSO) δ_{C} : 166.8 (C=O), 159.2 (C_{HAP-OH}), 158.9 (C_{Bzh-OH}), 158.7 (C=N), 14.5 (CH₃); CHN (% found (% calculated)): C 53.8 (52.9), H 4.8 (5.9), N 8.3 (8.2).

3.5.2 (BzyHAP-Br)



An ethanolic solution of 5-bromo-2-hydroxyacetophenone (1.1g, 5.0mmol) was added to a solution of 3, 5-dihydroxybenzohydrazide (0.8g, 5.0mmol). The mixture was refluxed for 2 hours. A pale brown precipitate formed was filtered, washed with ethanol, and dried. (40% yield); IR(ν_{\max} cm⁻¹): 1647 (C=O), 1618 (C=N), 1010 (N-N), 3277 (O-H), 3140 (N-H); ¹H NMR (ppm, 400 MHz, DMSO) δ_{H} : 13.5 (1H, s, H-N), 11.3 (1H, s, H-O_{HAP}), 9.6 (2H, s, H-O_{Bzh}), 7.7-6.4 (6H, m, H-Ar), 2.4 (3H, s, CH₃); ¹³C NMR (ppm, 100 MHz, DMSO) δ_{C} : 165.2 (C=O), 158.9 (C_{HAP-OH}), 158.4 (C_{Bzh-OH}), 156.9 (C=N), 14.6 (CH₃); CHN (% found (% calculated)): C 49.2 (49.3), H 3.6 (2.9), N 7.8 (7.7).

3.5.3 (BzyHAP-Cl)



A 3,5-dihydroxy-N'-[(5-chloro-2-hydroxyphenyl)methylidene]benzohydrazide was prepared by the condensation of 5-chloro-2-hydroxyacetophenone (0.9g, 5.0mmol) with 3,5-dihydroxybenzohydrazide (0.8g, 5.0mmol) in ethanol (50ml) achieved by boiling the mixture under reflux for 2 hours. The pale brown precipitate formed was filtered, washed with ethanol, and dried. (41% yield); IR(ν_{\max} , cm^{-1}): 1648 (C=O), 1619 (C=N), 1007 (N-N), 3293 (O-H), 3140 (N-H); ^1H NMR (ppm, 400 MHz, DMSO) δ_{H} : 13.4 (1H, s, H-N), 11.3 (1H, s, H-O_{HAP}), 9.6 (2H, s, H-O_{Bzh}), 7.6-6.4 (7H, m, H-Ar), 2.5 (3H, s, CH₃); ^{13}C NMR (ppm, 100 MHz, DMSO) δ_{C} : 165.2 (C=O), 158.9 (C_{HAP-OH}), 157.9 (C_{Bzh-OH}), 157.1 (C=N), 14.6 (CH₃); CHN (% found (% calculated)): C 56.0 (56.2), H 3.7 (4.1), N 8.8 (8.7).

Metal Complexes of Hydroxyacetophenone Benzohydrazone

3.5.4 Zn(BzyHAP-H)

A solution of 3,5-dihydroxy-N'-[(2-hydroxyphenyl)methylidene]benzohydrazide (1.4g, 5.0mmol) in ethanol(20 ml) was added to an ethanolic solution of Zinc acetate (0.5g, 2.5mmol) followed by a few drops of triethylamine, and the reaction mixture was refluxed for 5 hours. Yellowish precipitate formed was filtered, washed with ethanol, and air dried. (68%yield); IR($\nu_{\max}\text{cm}^{-1}$): 3298,3400 (O-H), 1602 (C=O), 1568 (C=N), 1010 (N-N), 573 (Zn-O), 424 (Zn-N) ; ^1H NMR (ppm, 400 MHz, DMSO) δ_{H} : 9.3 (2H, s, H-O_{Bzh}), 7.5-6.2 (7H, m, H-Ar), 2.6 (3H, s, CH₃); CHN (% found (% calculated)): C 48.8 (49.0), H 4.4 (3.8), N 7.5(7.6).

3.5.5 Zn(BzyHAP-Br)

The synthesis of *Zn(BzyHAP-Br)* employed in-situ reaction. First, an ethanolic solution of 5-bromo-2-hydroxyacetophenone (1.1g, 5.0mmol) was added to a solution of 3, 5-dihydroxybenzohydrazide (0.8g, 5.0mmol). The mixture was refluxed for 2 hours producing a brown solution. In the same flask, (0.5g, 2.5mmol) of Zinc acetate in 30ml ethanol was added drop wise, followed by a few drops of triethylamine. The reaction mixture was then refluxed for another 5 hours. Yellowish precipitate formed was filtered, washed with ethanol, and air dried. (90%yield). IR($\nu_{\max}\text{cm}^{-1}$): 3281,3519 (O-H), 1643 (C=O), 1596 (C=N), 1012 (N-N), 540 (Zn-O), 417 (Zn-N) ; ^1H NMR (ppm, 400 MHz, DMSO) δ_{H} : 9.2 (2H, s, H-O_{Bzh}), 7.4-6.2 (6H, m, H-Ar), 2.6 (3H, s, CH₃); CHN (% found (% calculated)): C 42.0 (42.0), H 3.6 (2.6), N 6.0 (6.5).

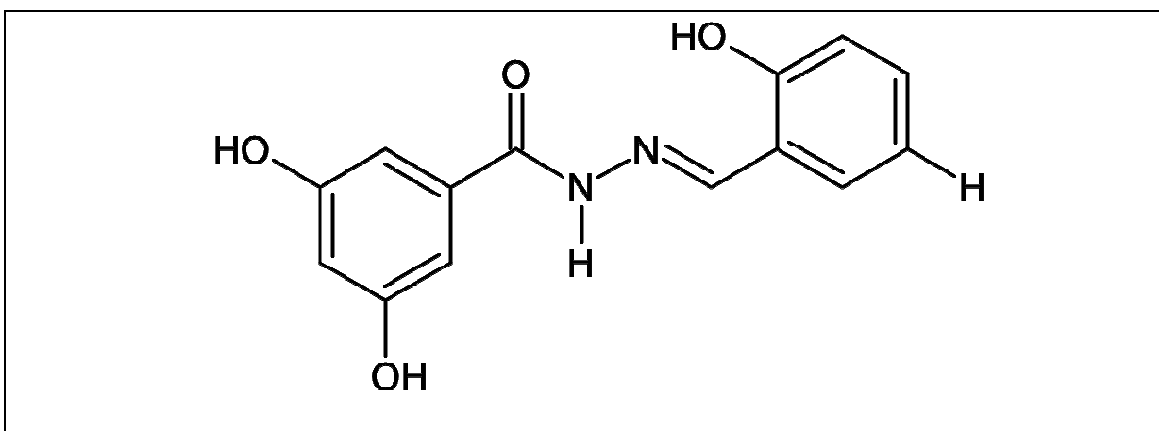
3.5.6 Zn(BzyHAP-Cl)

The synthesis of *Zn(BzyHAP-Cl)* employed in-situ reaction. First, an ethanolic solution of 5-chloro-2-hydroxyacetophenone (0.9g, 5.0mmol) was added to a solution of 3, 5-dihydroxybenzohydrazide (0.8g, 5.0mmol). The mixture was refluxed for 2 hours and gave a brown solution. In the same flask, (0.5g, 2.5mmol) of Zinc acetate in 30ml ethanol was added drop wise, followed by a few drops of triethylamine. The reaction mixture was then refluxed for another 5 hours. Yellowish precipitate formed was filtered, washed with ethanol, and air dried. (70%yield); IR($\nu_{\max}\text{cm}^{-1}$): 3287,3617 (O-H), 1601 (C=O), 1568 (C=N), 1011 (N-N), 587 (Zn-O), 481 (Zn-N) ; ^1H NMR (ppm, 400 MHz, DMSO) δ_{H} : 9.2 (2H, s, H- O_{Bzh}), 7.4-6.2 (6H, m, H-Ar), 2.6 (3H, s, CH_3); CHN (% found (% calculated)): C 43.1 (44.8), H 3.4 (3.3), N 7.2 (7.0).

3.6 Series 2: Salicylaldehyde Benzohydrazones

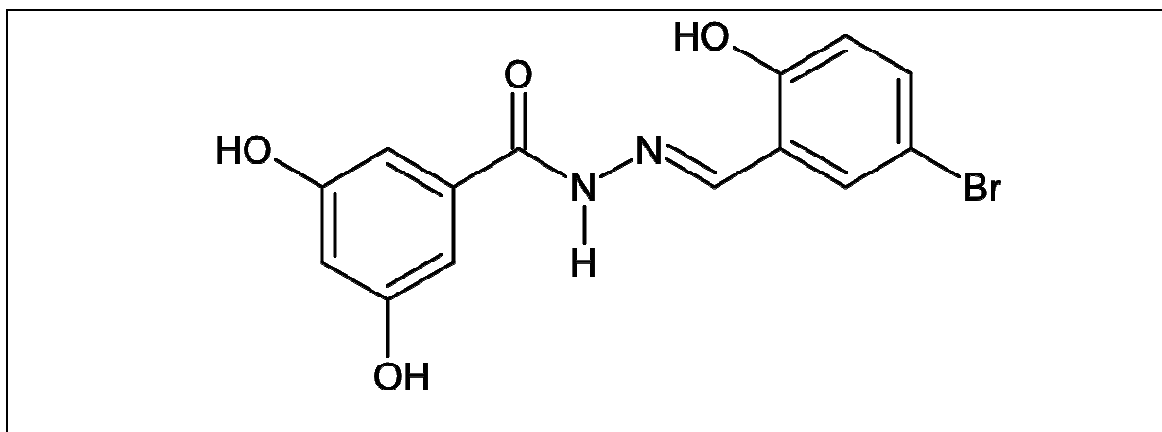
Synthesis of the ligands

3.6.1 (BzySAL-H)



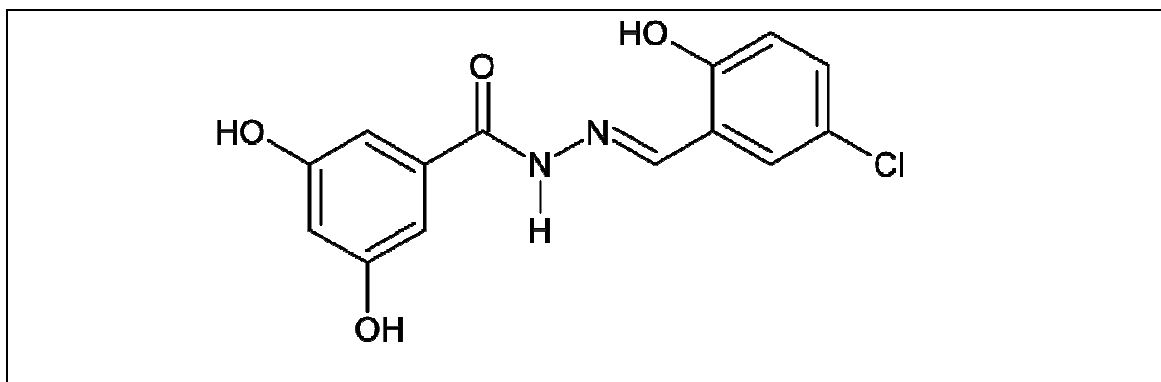
To a hot ethanolic solution of 3, 5-dihydroxybenzohydrazide (0.8g, 5.0mmol), salicylaldehyde (0.5ml, 5.0mmol) was added drop wise. The reaction mixture was refluxed for 2 hours. A pale brown precipitate formed was filtered, washed with ethanol, and dried in air. (40% yield); IR(ν_{\max} cm⁻¹): 1649 (C=O), 1591 (C=N), 1007 (N-N), 3384 (O-H), 3224 (N-H); ¹H NMR (ppm, 400 MHz, DMSO) δ_{H} : 11.9 (1H, s, H-N), 11.3 (1H, s, H-O_{SAL}), 9.6 (2H, s, H-O_{Bzh}), 8.6 (1H, s, H-C=N), 7.6-6.4 (7H, m, H-Ar); ¹³C NMR (ppm, 100 MHz, DMSO) δ_{C} : 163.5 (C=O), 159.0 (C_{SAL}-OH), 158.0 (C_{Bzh}-OH), 148.8 (C=N); CHN (% found (% calculated)): C 59.6 (60.7), H 4.4 (4.5), N 10.6 (10.3).

3.6.2 (BzySAL-Br)



In a 100ml round-bottom flask, 5-bromosalicylaldehyde (1.0g, 5.0mmol) was dissolved in 20ml ethanol. An ethanolic solution containing 3, 5-dihydroxybenzohydrazide (0.8g, 5.0mmol) was added, and the reaction was refluxed for 2 hours. The ethanol was evaporated and the crystals of *BzySAL-Br* were deposited over a period of few days. The solid was filtered, washed with ethanol, and air-dried. (80% yield); IR(ν_{\max} cm⁻¹): 1655 (C=O), 1591 (C=N), 990 (N-N), 3423 (O-H), 3209 (N-H); ¹H NMR (ppm, 400 MHz, DMSO) δ_{H} : 12.0 (1H, s, H-N), 11.3 (1H, s, H-O_{SAL}), 9.6 (2H, s, H-O_{Bzh}), 8.5 (1H, s, H-C=N), 7.7-6.4 (6H, m, H-Ar); ¹³C NMR (ppm, 100 MHz, DMSO) δ_{C} : 163.7 (C=O), 158.9 (C_{SAL}-OH), 156.9 (C_{Bzh}-OH), 146.2 (C=N); CHN (% found (% calculated)): C 45.4 (45.6), H 3.1 (2.7), N 7.7 (7.6).

3.6.3 (BzySAL-Cl)



An ethanolic solution of 5-chlorosalicylaldehyde (0.8g, 5.0mmol) was added to a solution of 3, 5-dihydroxybenzohydrazide (0.8g, 5.0mmol). The mixture was refluxed for 2 hours and gave a brown solution. Crystals of L6 were deposited over a period of few days. The solid was filtered, washed with ethanol, and air-dried. (74% yield); IR($\nu_{\max}\text{cm}^{-1}$): overlap (C=O), 1592 (C=N), 1000 (N-N), 3410 (O-H), 3210 (N-H); ^1H NMR (ppm, 400 MHz, DMSO) δ_{H} : 12.0 (1H, s, H-N), 11.3 (1H, s, H-O_{SAL}), 9.6 (2H, s, H-O_{Bzh}), 8.5 (1H, s, H-C=N), 7.6-6.4 (6H, m, H-Ar); ^{13}C NMR (ppm, 100 MHz, DMSO) δ_{C} : 163.7 (C=O), 158.9 (C_{SAL}-OH), 156.9 (C_{Bzh}-OH), 146.2 (C=N); CHN (% found (% calculated)): C 51.7 (51.8), H 3.2 (4.0), N 8.6 (8.7).

Metal Complexes of Salicylaldehyde Benzohydrazones

3.6.4 Cu(BzySAL-H)

Copper acetate (0.5g, 2.5mmol) dissolved in ethanol (20ml) was added slowly to a stirring solution of 3,5-dihydroxy-N'-[(2-hydroxyphenyl)ethylidene]benzohydrazide (1.4g, 5.0mmol) in 30ml ethanol. A few drops of triethylamine were added and the reaction mixture was refluxed for 5 hours. A green precipitate formed was filtered, washed with ethanol, and dried. (40% yield); IR($\nu_{\max}\text{cm}^{-1}$): 3299,3439 (O-H), 1603 (C=O), 1561 (C=N), 1009 (N-N), 601 (Cu-O), 490 (Cu-N) ; CHN (% found (% calculated)): C 45.9 (45.3), H 3.7 (4.1), N 7.7 (7.6).

3.6.5 Zn(BzySAL-H)

Zinc acetate (0.5g, 2.5mmol) was dissolved in ethanol (20 ml) and the solution was added dropwise to a hot ethanolic solution of 3,5-dihydroxy-N'-[(2-hydroxyphenyl)ethylidene]benzohydrazide (1.4g, 5.0mmol) followed by a few drops of triethylamine, and the reaction mixture was refluxed for 5 hours. Yellowish precipitate obtained was filtered, washed with ethanol, and air dried. (30%yield); IR($\nu_{\max}\text{cm}^{-1}$): broad (O-H), 1597 (C=O), 1576 (C=N), 1010 (N-N), 590 (Zn-O), 442 (Zn-N); ^1H NMR (ppm, 400 MHz, DMSO) δ_{H} : 9.0 (2H, s, H-O_{Bzh}), 8.6 (1H, s, H-C=N), 7.4-6.4 (7H, m, H-Ar); CHN (% found (% calculated)): C 54.8 (55.2), H 3.7 (3.8), N 8.7 (9.2).

3.6.6 Cu(BzySAL-Br)

To a solution of 3,5-dihydroxy-N'-[(5-bromo-2-hydroxyphenyl)ethylidene] benzohydrazide (1.8g, 5.0mmol) in 30ml of ethanol, an ethanolic solution of copper acetate (0.5g, 2.5mmol) was added drop wise followed by a few drops of triethylamine and the reaction mixture was refluxed for 5 hours. A green precipitate formed was filtered, washed with ethanol, and dried. (82% yield); IR($\nu_{\max}\text{cm}^{-1}$): 3401,3529 (O-H), 1605 (C=O), overlap (C=N), 1001 (N-N), 573 (Cu-O), 453 (Cu-N) ; CHN (% found (% calculated)): C 40.0 (40.7), H 2.9 (2.4), N 6.1 (6.8).

3.6.7 Zn(BzySAL-Br)

A solution of 3,5-dihydroxy-N'-[(5-bromo-2-hydroxyphenyl)ethylidene] benzohydrazide (1.8g, 5.0mmol) in ethanol (20 ml) was added to an ethanolic solution of Zinc acetate (0.5g, 2.5mmol) followed by a few drops of triethylamine, and the reaction mixture was refluxed for 5 hours. Yellowish precipitate formed was filtered, washed with ethanol, and air dried. (15%yield); IR($\nu_{\max}\text{cm}^{-1}$): 3422, broad (O-H), 1615 (C=O), 1581 (C=N), 1009 (N-N), 559 (Zn-O), 455 (Zn-N) ; ^1H NMR (ppm, 400 MHz, DMSO) δ_{H} : 9.0 (2H, s, H-O_{Bzh}), 8.5 (1H, s, H-C=N), 7.0-6.2 (6H, m, H-Ar); CHN (% found (% calculated)): C 40.1 (40.6), H 2.9 (2.2), N 6.9 (6.8).

3.6.8 Cu(BzySAL-Cl)

To a solution of 3,5-dihydroxy-N'-[(5-chloro-2-hydroxyphenyl)ethylidene] benzohydrazide (1.5g, 5.0mmol) in 30ml of ethanol, an ethanolic solution of copper acetate (0.5g, 2.5mmol) was added drop wise followed by a few drops of triethylamine and the reaction mixture was refluxed for 5 hours. A green precipitate formed was filtered, washed with ethanol, and dried. (20% yield); IR($\nu_{\max}\text{cm}^{-1}$): 3404, broad (O-H), 1610 (C=O), 1546 (C=N), 1010 (N-N), 574 (Cu-O), 457 (Cu-N) ; CHN (% found (% calculated)): C 45.9 (46.1), H 3.4 (3.9), N 6.0 (6.8).

3.6.9 Zn(BzySAL-Cl)

A solution of 3,5-dihydroxy-N'-[(5-chloro-2-hydroxyphenyl)ethylidene] benzohydrazide (1.5g, 5.0mmol) in ethanol (20 ml) was added to an ethanolic solution of Zinc acetate (0.5g, 2.5mmol) followed by a few drops of triethylamine, and the reaction mixture was refluxed for 5 hours. Yellowish precipitate formed was filtered, washed with ethanol, and air dried. (60%yield); IR($\nu_{\max}\text{cm}^{-1}$): 3359, broad (O-H), overlap (C=O), 1582 (C=N), 1010 (N-N), 565 (Zn-O), 452 (Zn-N) ; ^1H NMR (ppm, 400 MHz, DMSO) δ_{H} : 9.2 (2H, s, H- O_{Bzh}), 8.5 (1H, s, H-C=N), 7.0-6.2 (6H, m, H-Ar); CHN (% found (% calculated)): C 44.9 (45.4), H 2.9 (2.5), N 7.1 (7.2).

3.7 Experimental Procedures for Cytotoxicity Test.

3.7.1 Cell culture

All the cells that were used in this study were obtained from American Type Cell Collection (ATCC) and maintained in a 37⁰C incubator with 5% CO₂ saturation. HT-29 human colon adenocarcinoma cells and WRL-68 normal hepatic cells were maintained in Dulbecco's modified Eagle's medium (DMEM). Whereas A549 non-small cell lung cancer cells and PC3 prostate adenocarcinoma cells were maintained in RPMI medium. Both medium were supplemented with 10% fetus calf serum (FCS), 100 units/ml penicillin, and 0.1 mg/ml streptomycin.

3.7.2 MTT assay

Different cell lines types were used to determine the inhibitory effect of samples tested on cell growth using the MTT assay. This colorimetric assay is based on the conversion of the yellow tetrazolium bromide (MTT) to the purple formazan derivatives by mitochondrial succinate dehydrogenase in viable cells. For measurement of cell viability, cells were seeded at a density of 1×10^5 cells/ml in a 96-well plate and incubated for 24 hours at 37 °C, 5% CO₂. The next day, cells were treated with the test agents and incubated for another 24 hours. After 24 hours, MTT solution at 2 mg/ml was added for 1 hour. Absorbance at 570 nm were measured and recorded. Results were expressed as a percentage of control giving percentage cell viability after 24 hours exposure to test agent. The potency of cell growth inhibition for each test agent was expressed as an EC₅₀ value, defined as the concentration that caused a 50% loss of cell growth. Viability was defined as the ratio (expressed as a percentage) of absorbance of treated cells to untreated cells.

3.8 Experimental Procedures for Anti-oxidant Activity

3.8.1 DPPH assay

The DPPH (2,2-diphenylpicrylhydrazyl) radical scavenging activity effect of synthesized compounds was carried out according to the method described by Gorinstein (Gorinstein et al, 2003, Loo et al, 2007). 5 μ L of the tested compounds with a concentration range between 50-250 μ M were mixed with 195 μ L of 0.1 mM DPPH. An equal amount of methanol and DPPH served as control. After incubation in the dark for 20 min, absorbance was recorded at 517nm. The percentage of scavenging was calculated using the following equation:

$$\% \text{ scavenging} = (\text{Absorbance of control} - \text{Absorbance of sample}) / \text{Absorbance of control} \times 100\%$$

The total DPPH scavenging capacities of the ligands and complexes studied was measured and compared to Vitamin C and BHT.

3.8.2 FRAP Assay

The FRAP assay of the compounds performed using modified method as described by Benzie and Strain (Benzie et al., 1999) The stock solutions contained 300 mM acetate buffer (3.1 g CH₃COONa·3H₂O and 16 mL CH₃COOH), pH 3.6, 10 mM TPTZ (2,4,6-tripyridyl-*s*- triazine) solution in 40 mM hydrochloric acid and 20 mM ferric chloride hexahydrate solution. The fresh working solution was prepared by mixing acetate buffer (25 mL), TPTZ (2.5 mL), and ferric chloride hexahydrate solution (2.5 mL). The temperature of the solution was raised to 37 °C before use and allowed to react with the FRAP solution (300 μ L) in the dark. The colored product (ferrous tripyridyltriazine complex) was monitored at a wavelength of 593 nm. The standard curve was linear

between 100 and 1,000 μM ferrous sulphate. Results are expressed in μM ferrous/g dry mass and compared with that of ascorbic acid and butylated hydroxytoluene.

CHAPTER 4: RESULTS AND DISCUSSION

Two different series of ligands were prepared in this study of hydroxyacetophenone with benzohydrazone(BzyHAP) and salicylaldehyde with benzohydrazone(BzySAL). The series of BzyHAP ligands were synthesized by reacting the 3,5-dihydroxybenzohydrazide with 2-hydroxyacetophenone, 5-bromo-2-hydroxyacetophenone, and 5-chloro-2-hydroxyacetophenone while the other series engaged the reaction of the same benzohydrazone with salicylaldehyde, 5-bromosalicylaldehyde, and 5-chlorosalicylaldehyde. The (BzySAL) ligand were reacted with copper(II) salt and zinc(II) salt while the BzyHAP ligands undergo complexation with zinc(II) salt only.

All compounds were structurally elucidated by IR, ^1H NMR, and ^{13}C NMR spectral data and are supported by the results of elemental analysis. All Zn(II) complexes obtained are yellow while Copper(II) BzySAL is brown in colour. Cu(II) complexes of Br- and Cl-substituted BzySAL were appeared as green amorphous solid. The complexes are not soluble in common organic solvents, but most of them dissolve in dimethyl sulphoxide (DMSO).

4.1 Ligands and complexes of BzyHAP series

Table 4.1 shows the colours, yield and elemental analysis data of BzyHAP ligands and their Zn(II) complexes. The experimental data for elemental analyses is found to be in a good agreement with the proposed formulae as the values are approximately similar to each other. All the ligands and the Zn(II) complexes are pale white and yellow in colour respectively.

Table 4.1: Analytical data and physical properties of ligands and complexes of BzyHAP Series

Compound	Colour	Yield (%)	Elemental Percentage (%)		
			Found	Calculated	
BzyHAP-H	Pale white	41	53.8(52.9)	4.8(5.9)	8.3(8.2)
Zn(BzyHAP-H)	Yellow	30	48.8(49.0)	4.4(3.8)	7.5(7.6)
BzyHAP-Br	Pale white	41	49.2(49.3)	3.6(2.9)	7.8(7.7)
Zn(BzyHAP-Br)	Pale yellow	90	42.0(42.0)	3.6(2.6)	6.0(6.5)
BzyHAP-Cl	Pale white	15	56.0(56.2)	3.7(4.1)	8.8(8.7)
Zn(BzyHAP-Cl)	Yellow	40	43.1(44.8)	3.4(3.3)	7.2(7.0)

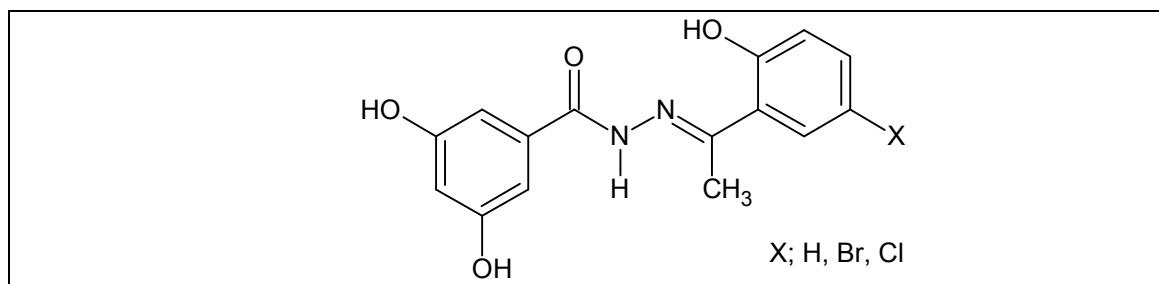


Figure 4.1: BzyHAP series ligand

4.1.1 IR Spectral Data

The important stretching and bending frequencies of the IR spectra of the ligands and their Zn(II) complexes are tabulated in table 4.2.

The infrared spectra (IR) provide valuable information of the functional groups of the studied compounds. The coordination of the ligand to the metal center could be determined by comparing the IR spectra of the metal complexes with their respective ligands and are mainly elucidated by the shifting of imine $\nu(\text{C}=\text{N})$ signal and the formation of new metal-oxygen $\nu(\text{M}-\text{O})$ and metal-nitrogen $\nu(\text{M}-\text{N})$ bands. Nonetheless, the assignment of M-O and M-N bands at the lower region seems to be intricate due to the interference with the vibration signals of the ligand. In addition, N-H stretching band could not be easily assigned due to the overlapping with OH broad signals.

The strong and the medium intensity broad band displayed at higher frequency around $3277\text{-}3314\text{ cm}^{-1}$ is assigned to $\nu(\text{O}-\text{H})$ vibrations. The sharpness of the signals reveals that no intramolecular or intermolecular hydrogen bonding interaction occurs (Pouralimardan et al., 2007). The exhibition of a strong or a medium stretching band at a range of $1611\text{-}1619\text{ cm}^{-1}$ is attributable to the azomethine ($\text{C}=\text{N}$) (Nishata et al., 2010, Khuhawar et al., 2004).

The stretching band of (N-H) that exhibits at $3120\text{-}3140\text{ cm}^{-1}$ and the appearance of $\nu(\text{C}=\text{O})$ band assigned at $1642\text{-}1648\text{ cm}^{-1}$ (Pavia et al., 2009) indicates that the ligands exist in the keto form in solid state. Nevertheless, as both in solution and in the presence of metal ions, the compounds might exist in tautomeric enol form at equilibrium (Iskander et al., 2000).

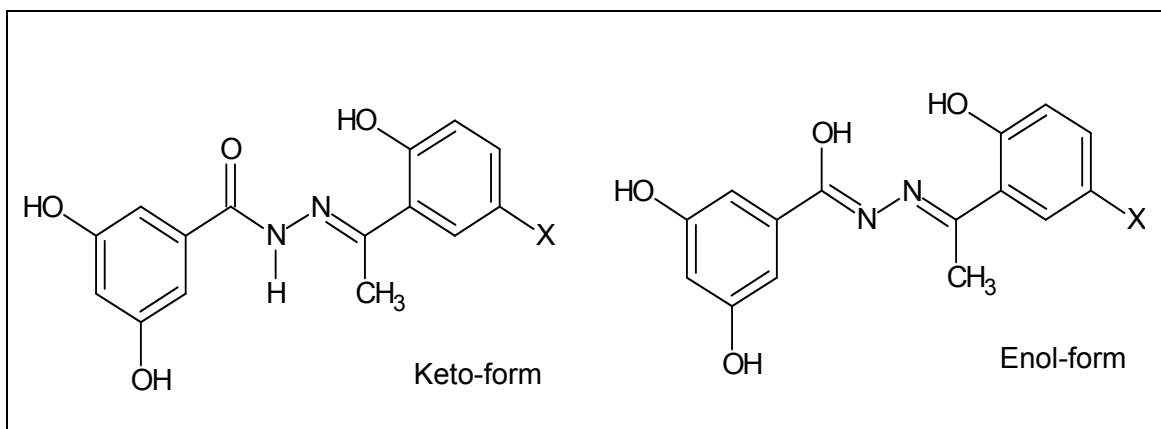


Figure 4:2: The keto and enol structure of the ligand

In the spectra of the complexes, $\nu(\text{C}=\text{N})$ band signal which shifted to the lower frequencies indicating that the coordination of the ligand to metal ion occurs through nitrogen atom of the imine group (Li et al., 2011). The bond formation of $\text{C}=\text{N}$ to metal ion is also supported by the positive shift of $\nu(\text{N}-\text{N})$ band about 10cm^{-1} (Chohan et al., 2002) that takes place due to the repulsion between lone pairs of electron belongs to the nitrogen caused by the coordination to metal center (Ali et al., 2003). The carbonyl $\nu(\text{C}=\text{O})$ band shifted to the lower frequency by 4 to 46cm^{-1} signifying the involvement of carbonyl oxygen atom in the formation of metal complex (Nagano et al., 1964). The shift of $\nu(\text{C}-\text{O})$ band by 4 to 22cm^{-1} suggesting the coordination via phenolic oxygen atom (Samus et al., 2002).

The disappearance of $\nu(\text{N}-\text{H})$ stretching band upon complexation, suggesting deprotonation and enolization of the ligand has occurred (Juahir et al., 2009).

Two new weak bands appears at lower frequencies range of $587\text{-}590\text{cm}^{-1}$ and $424\text{-}440\text{cm}^{-1}$ assigned to $\nu(\text{M}-\text{O})$, and $\nu(\text{M}-\text{N})$ respectively (Bagihalli et al., 2008), are observed in metal complexes spectra but not in the spectra of the ligand and consistent with the formation of the desired metal complexes. The presence of hydrates was characterized by the exhibition of bands in the range of $3400\text{-}3617\text{cm}^{-1}$ (Chan et al.,

1995). From IR spectra, it may be concluded that the ligands are tridentate, coordinated to metal ion via phenolic oxygen, imine nitrogen and carbonyl nitrogen atom.

Table 4.2: Selected IR Spectral Data of BzyHAP Series

Compound	Wavenumber (cm ⁻¹)							
	O-H	N-H	C=O	C=N	C-O	N-N	M-O	M-N
BzyHAP-H	3314	broad	1642	1611	1540, 1246	1003	-	-
Zn(BzyHAP-H)	3298, 3400	-	1602	1568	buried, 1242	1010	573	424
BzyHAP-Br	3277	3140	1647	1618	1523, 1247	1007	-	-
Zn(BzyHAP-Br)	3281, 3519	-	1643	1596	1530, 1225	1012	540	417
BzyHAP-Cl	3293	3140	1648	1619	1524, 1247	1007	-	-
Zn(BzyHAP-Cl)	3287, 3617	-	1601	1568	buried, 1226	1011	587	481

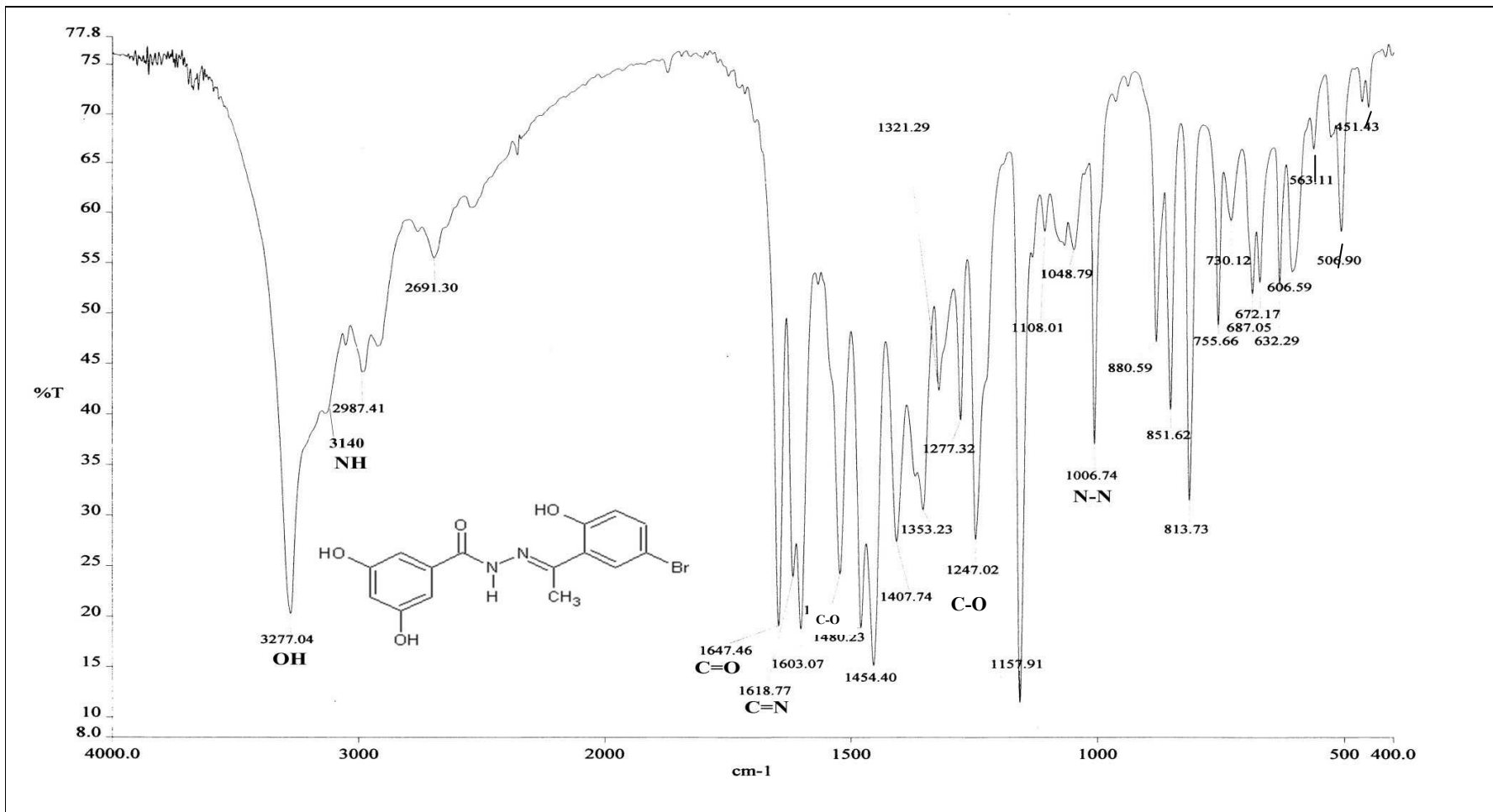


Figure 4.3: IR Spectra of BzyHAP-Br

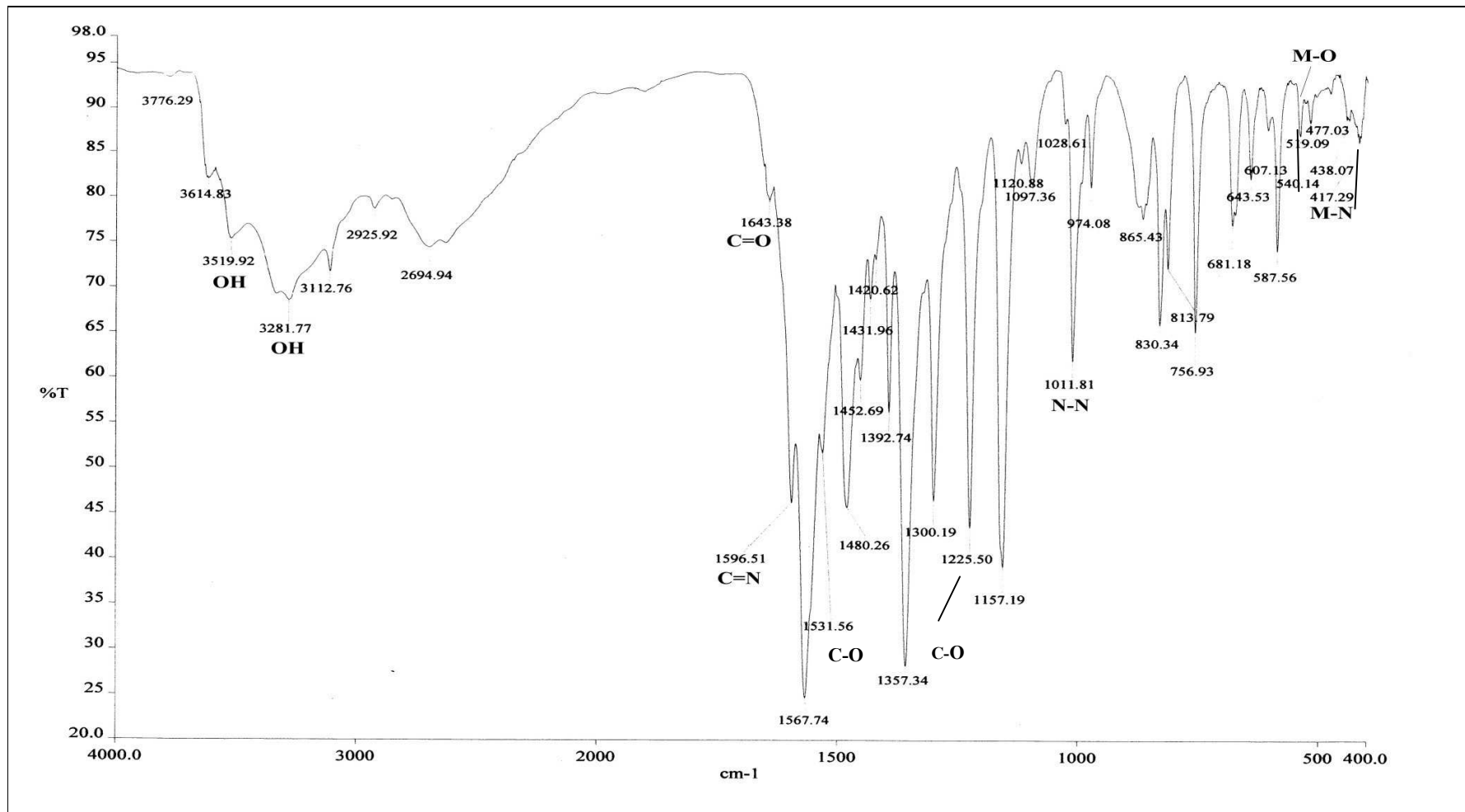


Figure 4.4: IR Spectra of Zn(BzyHAP-Br)

4.1.2 ¹H NMR Spectral Data

The ¹H NMR spectrum of BzyHAP Series ligands and their Zn(II) complexes were recorded in dimethyl sulphoxide (DMSO) with trimethylsilane (TMS) as internal standard. The chemical shifts are expressed in ppm, as depicted in table 4.3, followed by the hydrogen numbering scheme in figure 4.5.

Generally, five types of hydrogen are observed in the spectrum of ligands. A singlet downfield peak with integration due to one hydrogen atom is observed as the most deshielded at 13.4-13.5 ppm attributable to the proton attached to N-H¹ (Ferrari et al., 1999). The presence of δ(N-H) peak indicates that the free ligand employed keto form in solution (Iskander et al., 2000). The hydroxyl proton of hydroxyacetophenone (H²) exhibits a single downfield peak at 11.3 ppm and corresponds to one proton. A singlet peak resonates at 9.6-9.7ppm is assigned to the proton of dihydroxy moiety of the benzohydrazone (H³). The methyl-H⁵ band resonates at the most upperfield and the integration value is due to three hydrogen atoms, while multiplet signals lying on the range of 6.4-7.7 of the ¹H NMR spectrum are assigned to aromatic hydrogen. These aromatic protons are deshielded by the large anisotropic field generated by the circulation of π-electrons in the ring (Pavia et al., 2001). The agreement of the data obtained from the ¹H NMR and the proposed structure indicates that the ligands are successfully synthesized.

The spectrum of Zn(II) complexes of the ligands show the disappearance of two bands previously assigned to proton of (N-H¹) and O-H² of hydroxyacetophenone moiety. The absence of O-H² proton is caused by the formation of a new Zn-O bond via the phenolic oxygen atom. The elimination of the proton belongs to N-H group demonstrates that the formation of a new Zn-O bond in which the ligand employs the enolic form (Ali et al.,

2003). The spectrum also shows very slight upfield shifts of benzohydrazone OH proton band by 0.4-0.6ppm while the resonance signals of the aromatic protons remain unchanged.

In summary, the deprotonation of N-H¹ demonstrate that in complexation, the ligands are in enolic form. In addition, the disappearance of phenolic proton indicates the ligands also coordinate to metal(II) ion through the hydroxy group of the hydroxyacetophenone. Thus, the ligands are most likely to function as tridentate ligands.

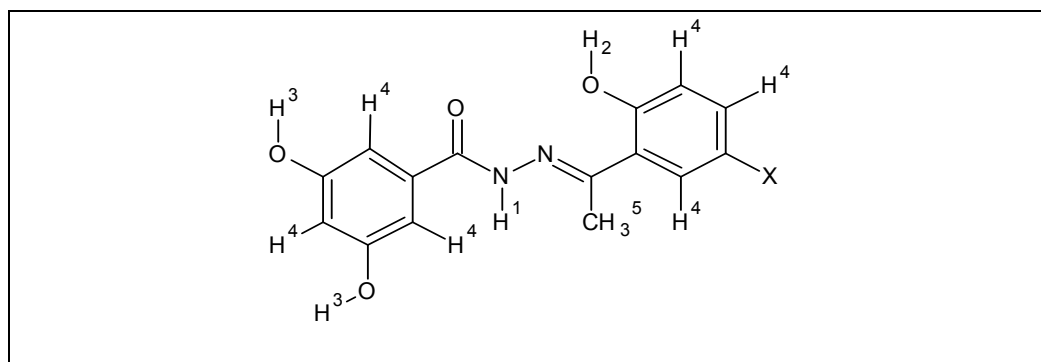


Figure 4.5: Proton numbering scheme of BzyHAP Series ligands

Table 4.3: ¹HNMR Spectral Data of BzyHAP Series and their Zn(II) complexes

Compound	Chemical Shift (ppm)				
	H ¹	H ²	H ³	H ⁴	H ⁵
BzyHAP-H	13.4	11.3	9.7	6.4-7.6	2.4
Zn(BzyHAP-H)	-	-	9.3	6.2-7.5	2.6
BzyHAP-Br	13.5	11.3	9.6	6.4-7.7	2.4
Zn(BzyHAP-Br)	-	-	9.2	6.2-7.4	2.6
BzyHAP-Cl	13.4	11.3	9.6	6.4-7.6	2.5
Zn(BzyHAP-Cl)	-	-	9.2	6.2-7.4	2.6

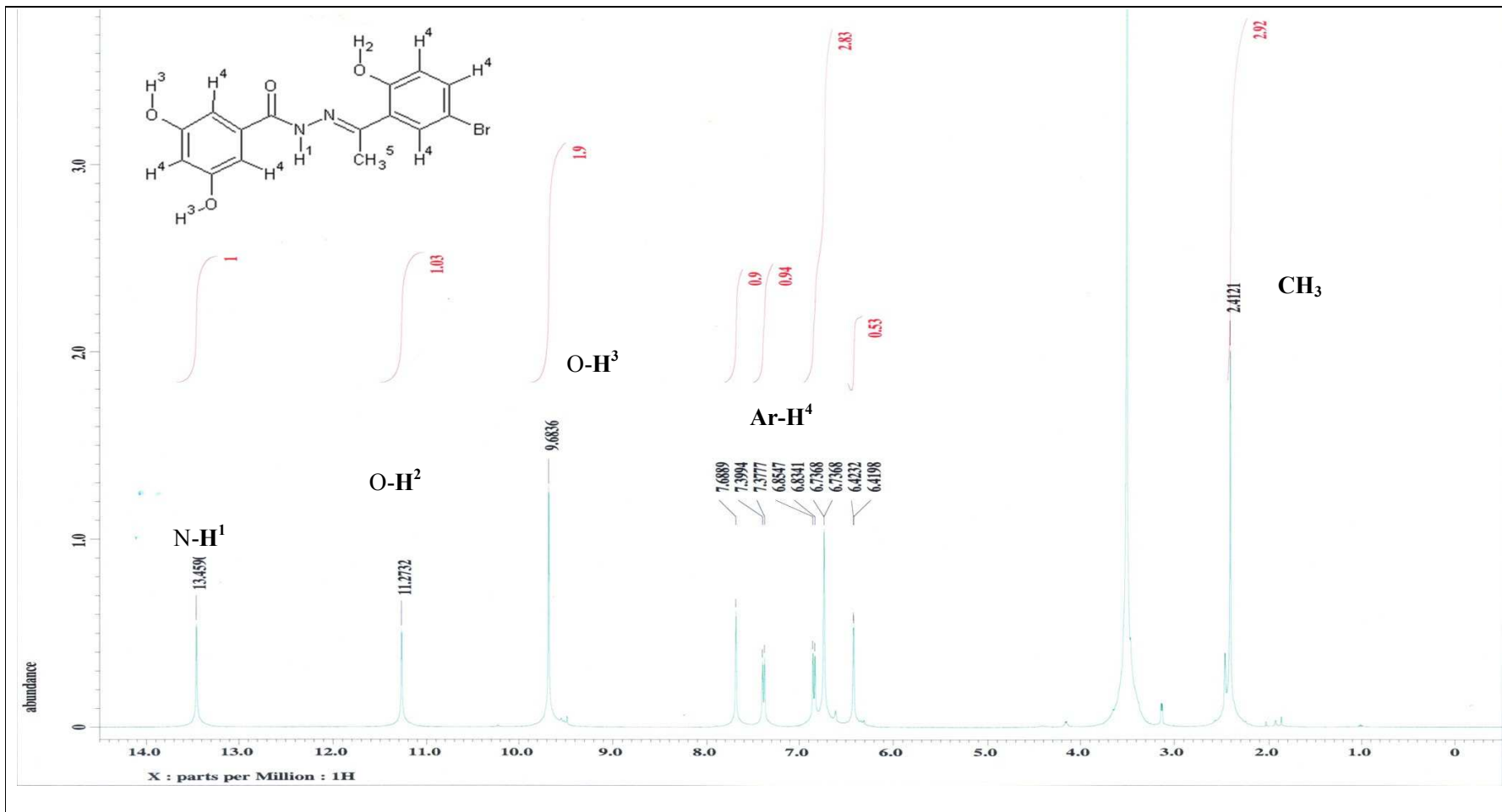


Figure 4.6: ^1H NMR Spectra of (BzyHAP-Br)

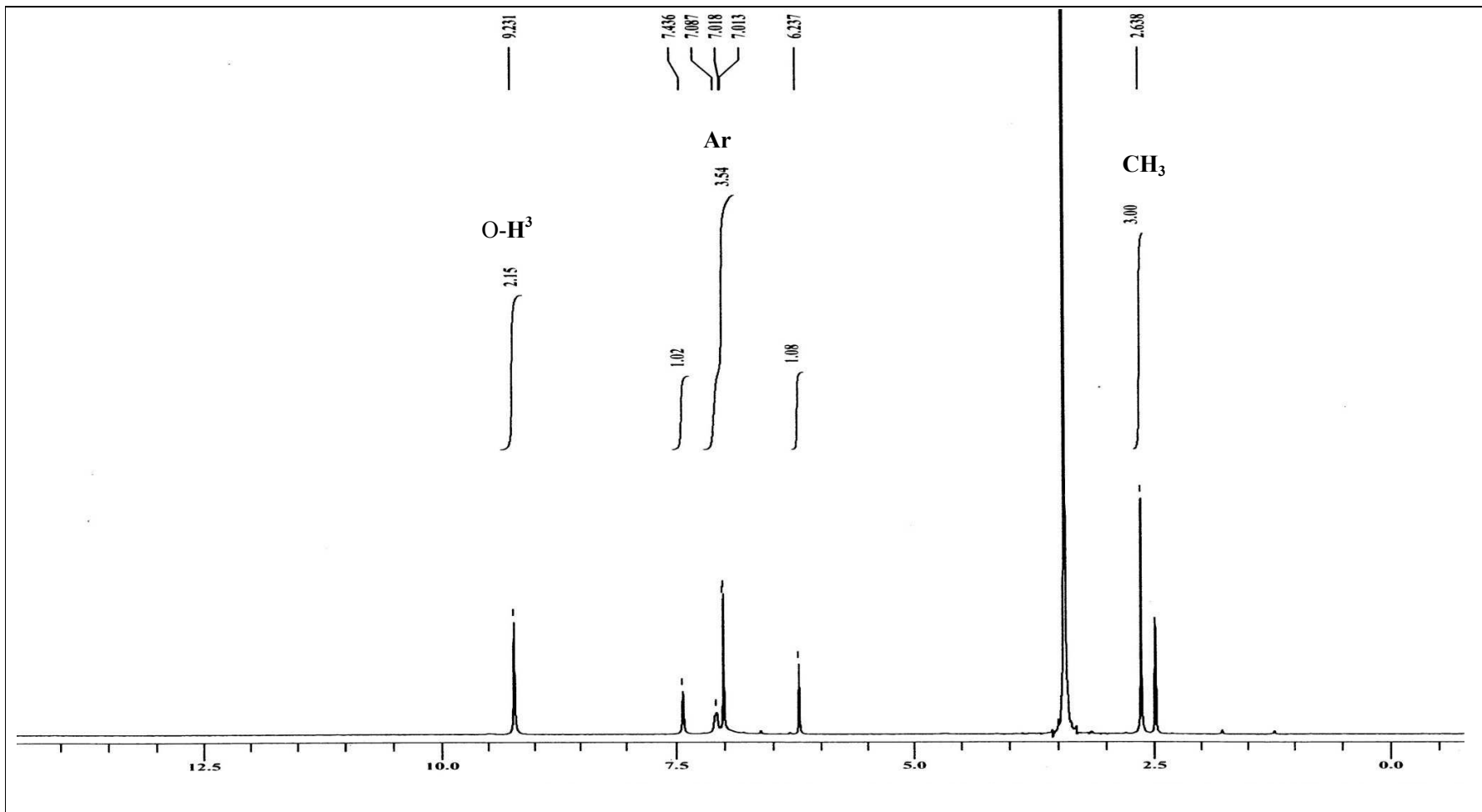


Figure 4.7: ¹H NMR Spectra of Zn(BzyHAP-Br)

4.1.3 ^{13}C NMR Spectral Data

The ^{13}C NMR spectrum of BzyHAP series ligands are summarized in table 4.4 and the full spectrum is shown in figure 4.9.

The spectrum displays 13 signals correspond to 13 different types of carbon, thus in agreement with the proposed structures. The $\delta(\text{C}^1=\text{O})$ signal appears at the most downfield due to the electronegative effect of the oxygen directly attached to it and the sp^2 hybridization (Pavia et al., 2001).

The peaks resonate at downfield of 158.9-159.2 ppm and 157.9-158.9 ppm are assigned to hydroxyl carbon of benzohydrazone ($\text{C}^2\text{-OH}$) and hydroxyacetophenone ($\text{C}^3\text{-OH}$) moiety respectively. The azomethine ($\text{C}^4=\text{N}$) carbon signal is observed at 156.9-158.7 ppm and the peaks of aromatic carbons laid at the range of 104.8-139.1 ppm of the spectrum. The aliphatic carbons resonate at the greatest upfield

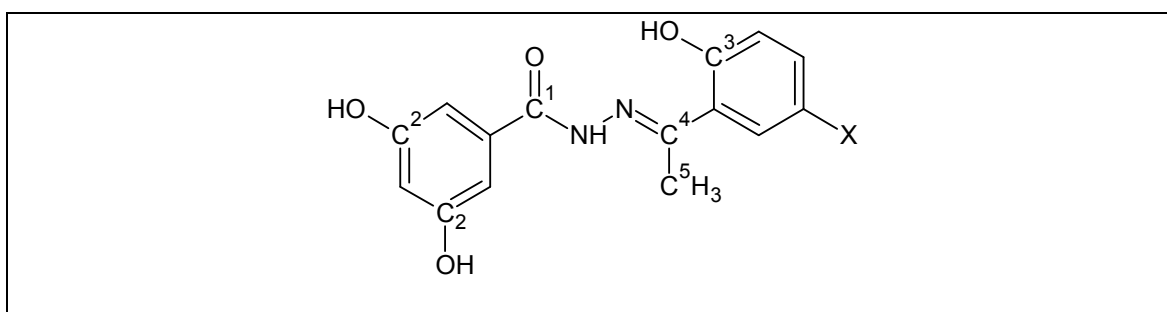


Figure 4.8: Carbon numbering scheme of BzyHAP Series ligands

Table 4.4: ^{13}C NMR Spectral Data of BzyHAP Series

Compound	Chemical Shift (ppm)					
	$\text{C}^1=\text{O}$	$\text{C}^2\text{-OH}$	$\text{C}^3\text{-OH}$	$\text{C}^4=\text{N}$	Ar-C	$\text{C}^5\text{-H}_3$
BzyHAP-H	166.8	159.2	158.9	158.7	105.5-136.0	14.5
BzyHAP-Br	165.2	158.9	158.4	156.9	106.5-135.2	14.6
BzyHAP-Cl	165.2	158.9	157.9	157.1	104.8-139.1	14.6

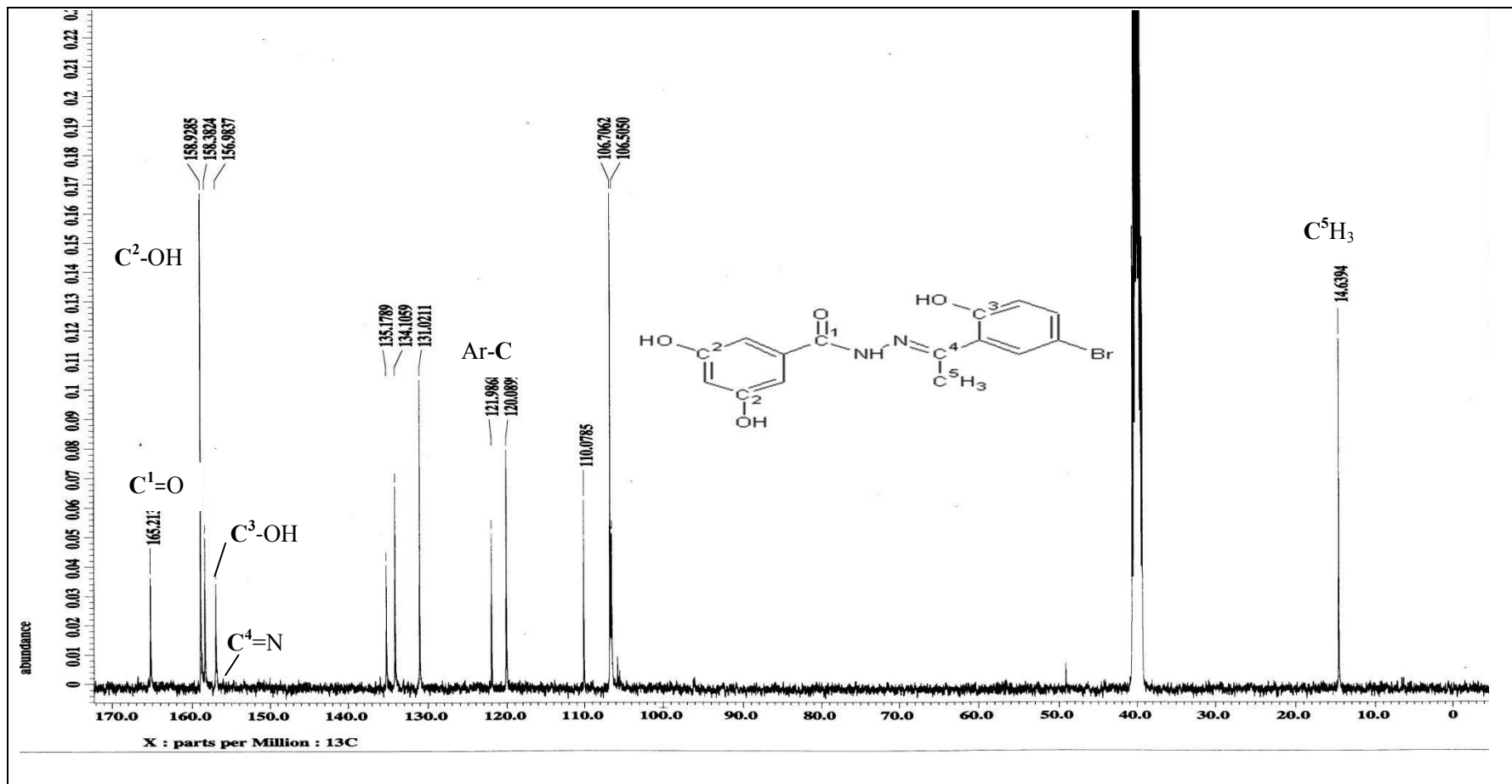


Figure 4.9 ^{13}C NMR Spectral of BzyHAP-Br

4.1.4 UV-Vis Spectral Data

The electronic absorption spectrum of the ligands and their Zn(II) complexes were recorded at 200-800nm in dimethyl sulphoxide (DMSO) and the data attained is tabulated in table 4.5.

In the free ligand, the spectrum is expected to exhibit two characteristic bands that represent the $\pi \rightarrow \pi^*$ transition originating from aromatic rings and $n \rightarrow \pi^*$ transition of azomethine (-NH-N=C-) group. The formation of the metal complexes is demonstrated by the appearance of new intense (LMCT) band due to the charge transfer transition from the lone pair of phenolate oxygen to metal ion and the blue shift of the $\pi \rightarrow \pi^*$ transition and $n \rightarrow \pi^*$ transition bands to higher frequency (Golcu et al., 2005) The spectrum of the ligands displays the band centered at 261-287nm assignable to $\pi \rightarrow \pi^*$ transition of aromatic rings (Bosnich, 1968). The electrons of imine group give rise to the $n \rightarrow \pi^*$ transition peak centered at 295-334nm in the spectrum.

With respect to the coordination of the free ligand to Zn(II) ion center, the spectra exhibit three main bands. Both $\pi \rightarrow \pi^*$ and $n \rightarrow \pi^*$ transition bands experience hypsochromic shift and appear at the shorter wavelength of 209-261nm and 259-310nm respectively. The exhibition of the new LMCT band centered at 302-397nm is associated with the charge transfer in the spectra of metal complexes supported the formation of the Zinc(II) complexes (Garnier-Suillerot et al., 1981). As expected, d-d transitions do not exist for d^{10} system of Zn(II) complexes.

Table 4.5: UV-Vis Spectral Data of BzyHAP Series and their Zn(II) complexes

Compound	Wavelength (nm)		
	$\pi \rightarrow \pi^*$	$n \rightarrow \pi^*$	LMCT
BzyHAP-H	261	295	-
Zn(BzyHAP-H)	209	259	302
BzyHAP-Br	288	332	-
Zn(BzyHAP-Br)	241	263	307
BzyHAP-Cl	287	334	-
Zn(BzyHAP-Cl)	265	310	397

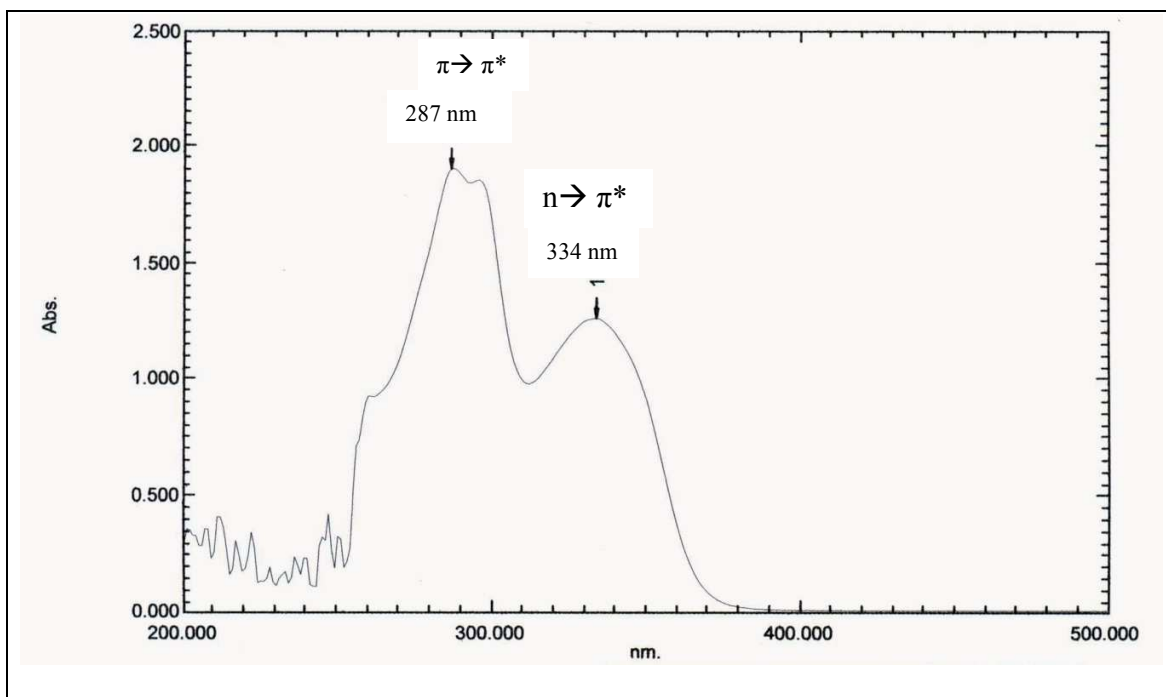


Figure 4.10 UV Spectra of BzyHAPCl

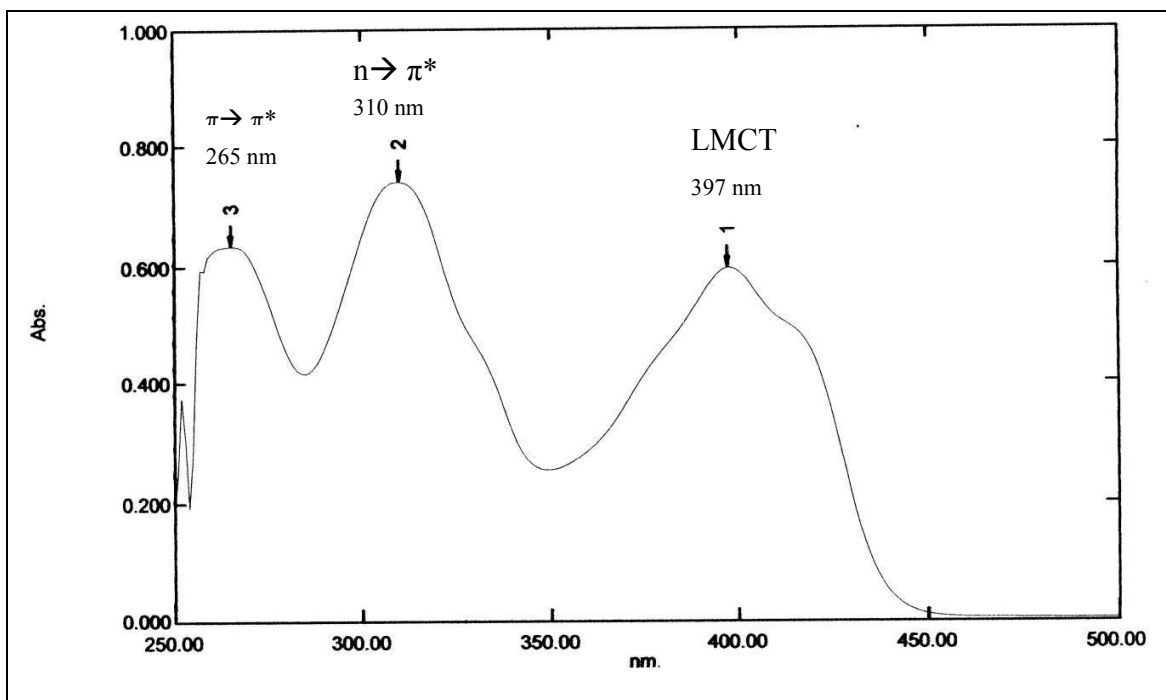


Figure 4.11 UV Spectra of ZnBzyHAPCl

4.1.5 Metal analysis by Atomic Absorption Spectroscopy (AAS)

Acid digestion method ASTM3005 (American Society for Testing Material) with some modification was employed to analyse the metal composition of complexes.

Firstly, the sample was weighted accurately before the addition of 2ml of concentrated nitric acid followed by 5ml of concentrated hydrochloric acid. The mixture was then heated on the hot plate until the solution became clear. The solution was allowed to cool, and adjusted to final volume 100ml with distilled water. The sample was replicated by diluting 0.5ml of stock solution to the final volume of 25ml. The experimental composition of the metal was calculated as follows:

$$\text{Experimental metal composition (\%)} = (\text{concentration (ppm)} \times 0.25) / \text{mass used}$$

The results obtained from the analysis are summarized in table 4.6. The experimental metal composition and the theoretical percentage of the proposed structures show a good agreement indicating the formation of the desired complexes.

Table 4.6: Experimental and Theoretical Metal Composition of the Zn(II) complexes

Compound	Mass used(g)	Concentration (mg/L)	Experimental metal	Theoretical metal
Zn(BzyHAP-H)	0.0090	0.286	15.89	17.79
Zn(BzyHAP-Br)	0.0233	0.583	12.51	15.26
Zn(BzyHAP-Cl)	0.0198	0.627	15.83	16.27

4.1.6 Proposed Structures of BzyHAP Series and their Zn(II) complexes

The spectroscopic and elemental analyses of the compounds make a good agreement with the proposed structural formula of the ligands.

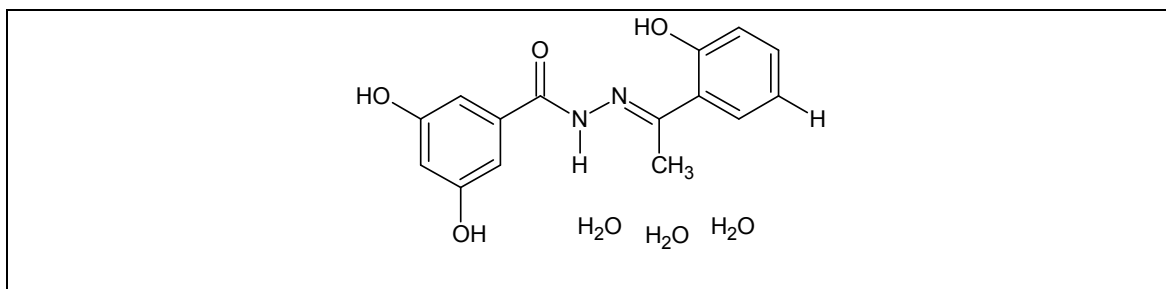


Figure 4.12: Proposed structure of BzyHAP-H

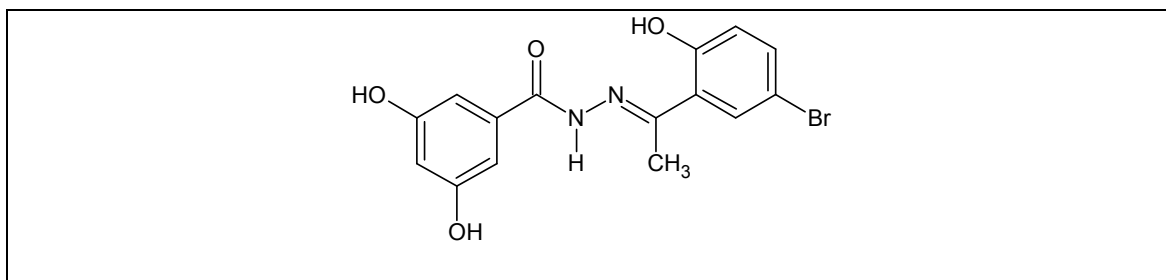


Figure 4.13: Proposed structure of BzyHAP-Br

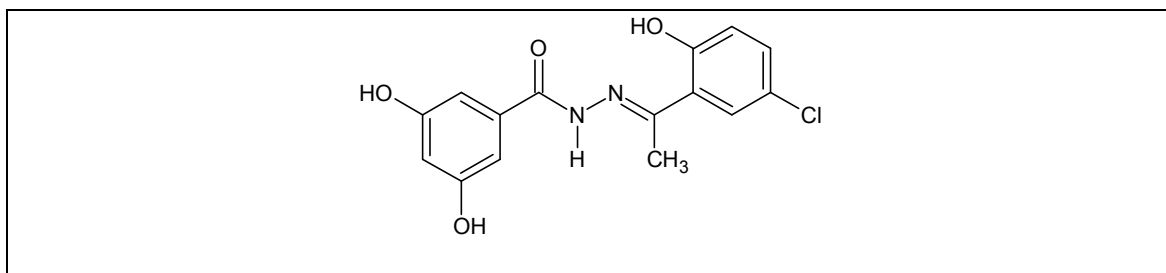


Figure 4.14: Proposed structure of BzyHAP-Cl

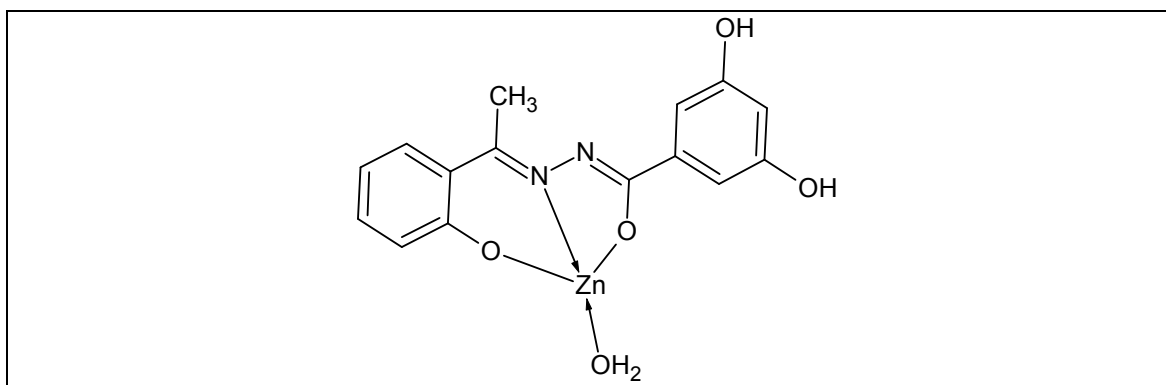


Figure 4.15: Proposed structure of Zn(BzyHAP-H)

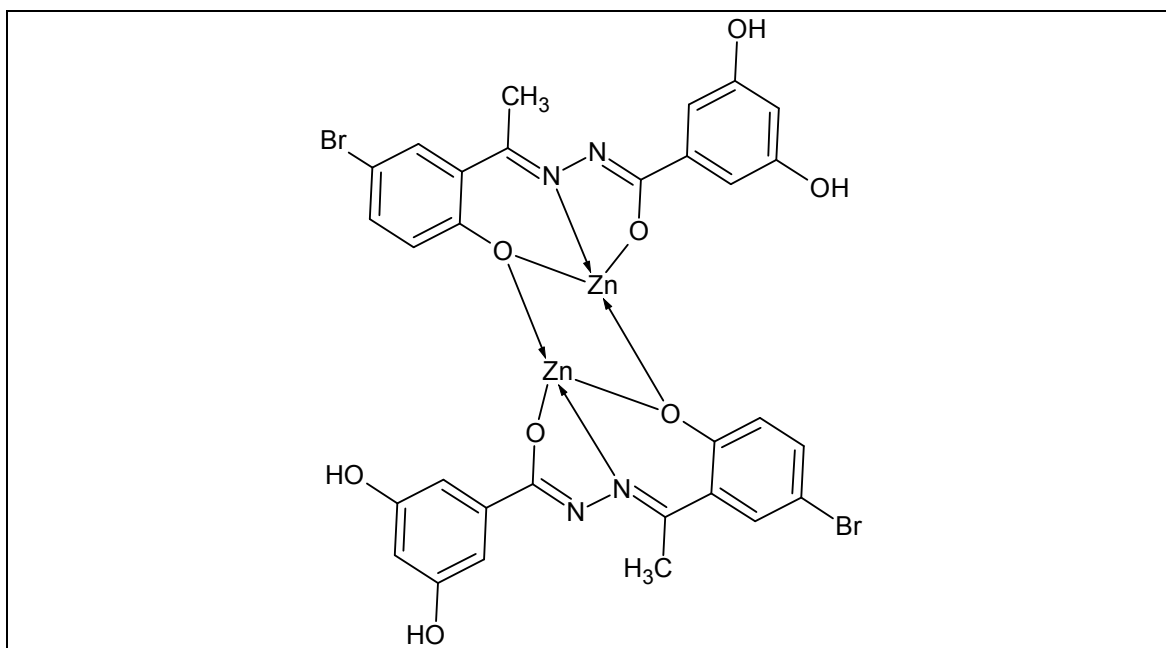


Figure 4.16: Proposed structure of Zn(BzyHAP-Br)

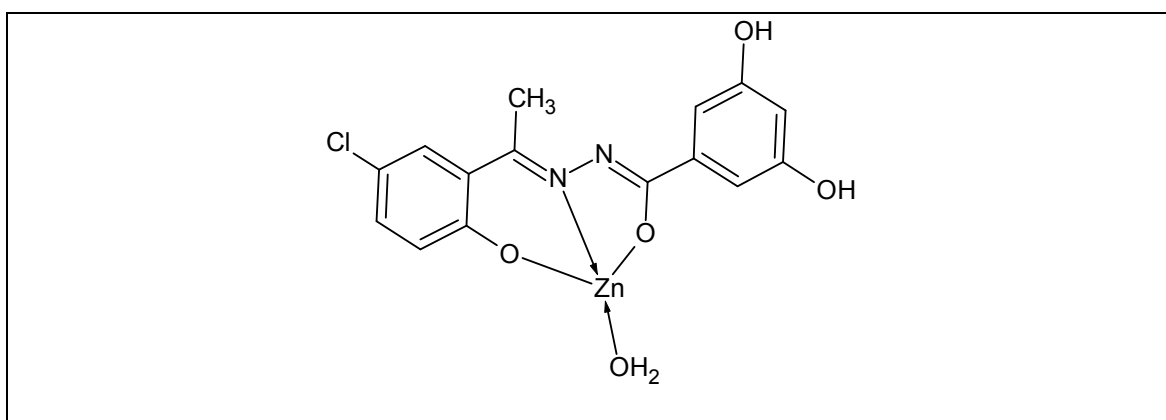


Figure 4.17: Proposed structure of Zn(BzyHAP-Cl)

4.2 Ligands and complexes of BzySAL Series

Table 4.7 shows the colours, yield and elemental analysis data of BzySAL ligands and their Cu(II), and Zn(II) complexes. The experimental data is found to be in a good agreement with the proposed formulae as the values are approximately similar to each other. All the ligands are pale white, the Zn(II) complexes are yellow, Cu(BzySAL-Br) and Cu(BzySAL-Cl) appears as green solid while Cu(BzySAL-H) is brown in colour.

Table 4.7: Analytical data and physical properties of ligands and complexes of BzySAL Series

Compound	Colour	Yield (%)	Elemental Percentage (%)		
			Found	(Calculated)	
			C	H	N
BzySAL-H	Pale white	40	59.6(60.7)	4.4(4.5)	10.6(10.3)
Cu(BzySAL-H)	Brown	40	45.9(45.3)	3.7(4.1)	7.7(7.6)
Zn(BzySAL-H)	Yellow	30	54.8(55.2)	3.7(3.8)	8.7(9.2)
BzySAL-Br	Pale white	80	45.4(45.6)	3.1(2.7)	7.7(7.6)
Cu(BzySAL-Br)	Green	82	40.0(40.7)	2.9(2.4)	6.1(6.8)
Zn(BzySAL-Br)	Yellow	14	40.1(40.6)	2.9(2.2)	6.9(6.8)
BzySAL-Cl	Pale white	74	51.7(51.8)	3.2(4.0)	8.6(8.7)
Cu(BzySAL-Cl)	Green	78	45.9(46.1)	3.4(3.9)	6.0(6.8)
Zn(BzySAL-Cl)	Yellow	28	44.9(45.4)	2.9(2.5)	7.1(7.2)

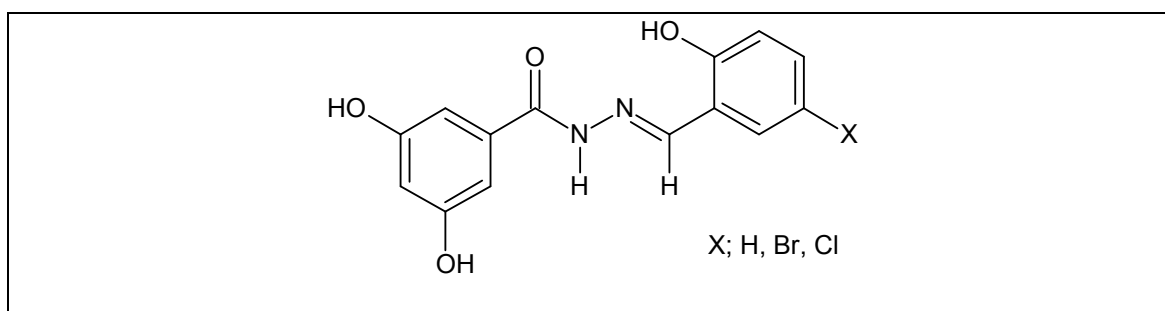


Figure 4.18: BzySAL series ligand

4.2.1 IR Spectral Data

The assignment of the important IR data of the BzySAL series ligands, and their Cu(II) and Zn(II) complexes is shown in table 4.8.

The spectra of free ligands and their respective Cu(II) and Zn(II) complex have been compared to investigate the formation metal-ligand bond. The IR spectrum for the complexes includes all the absorption bands belong to the ligands and some new bands correspond to the formation of the metal-ligand bond. The ligand may act as a tridentate ligand coordinating via imine nitrogen, phenolic oxygen and carbonyl oxygen (Lu et al., 2006), thus the assignment of the spectra band has been carried out according to the signal change of possible involved binding. Nonetheless, the interference of the vibrational signals of the ligands, complicates the assignment of the band newly formed $\nu(\text{M-O})$ and $\nu(\text{M-N})$ bands. The determination of N-H stretching band could not be easily assigned due to the overlapping with OH broad signals (Chan et al., 1995).

The spectra of the ligands show the exhibition of a strong or medium stretching band at a range of $1590\text{-}1591\text{ cm}^{-1}$ attributable to the new azomethine (C=N) group that formed via condensation of benzohydrazone and salicylaldehyde (Ran et al., 2010). The appearance of $\nu(\text{C=O})$ band assigned at 1649cm^{-1} and 1655 cm^{-1} in the spectra of BzySAL-H and BzySAL-Br respectively, indicates that the ligands exist in the keto form in solid state (Mohan et al., 1987). However, the signal for BzySAL-Cl is overlapped with the newly formed imine peak. In addition, the exhibition of $\nu(\text{N-H})$ peak at $3209\text{-}3224\text{ cm}^{-1}$ suggesting that the ligands behave in keto form in solid state. The $\nu(\text{O-H})$ vibrational band, employed either strong or medium broad peak, exhibits at higher frequency of $3384\text{-}3423\text{ cm}^{-1}$ (Mashaly et al., 2004).

The metal-nitrogen coordination is demonstrated by the negative shift of $\nu(\text{C}=\text{N})$ band to lower frequencies (Demir et al., 2005) suggesting coordination through nitrogen atom of the azomethine. It is also supported by the positive shift of $\nu(\text{N}-\text{N})$ band to the higher frequency indicating coordination of one nitrogen of the N-N group (Singh et al., 2008). The involvement of the carbonyl group in the coordination is confirmed by the shift of the band to a slightly lower frequency (Sharma et al., 2001). The absence of bands due $\nu(\text{C}=\text{O})$ and $\nu(\text{N}-\text{H})$ stretching vibration in $\text{Zn}(\text{BzySAL}-\text{Br})$ and $\text{Zn}(\text{BzySALCl})$ complexes suggesting the coordination of the carbonyl group in enolic form as the result of keto-enol or amide-imidol tautomerism (Jayabalakrisnan et al., 2003).

Further conclusive idea of the complexation is shown by the appearance of two new weak bands at the lower frequencies range of $559-601\text{ cm}^{-1}$ and $442-490\text{ cm}^{-1}$ assigned to $\nu(\text{M}-\text{O})$, and $\nu(\text{M}-\text{N})$ (Temel et al., 2004) respectively, indicating the coordination to metal ion via deprotonated phenolic oxygen and azomethine nitrogen atom (Nakamoto, 1978). The stretching band of $\nu(\text{O}-\text{H})$ experiences negative shift to lower frequency by $22-85\text{ cm}^{-1}$ along with exhibition of new $\nu(\text{O}-\text{H})$ at higher frequency indicating the presence of coordinated water in the complexes (Singh K. et al., 2006).

In summary, the ligands are found to coordinate to metal ion via phenolic oxygen, imine nitrogen and carbonyl nitrogen atom.

Table 4.8: Selected IR Spectral Data of BzySAL Series and their Cu(II) and Zn(II) complexes

Compound	Wavenumber (cm ⁻¹)							
	O-H	N-H	C=O	C=N	C-O	N-N	M-O	M-N
BzySAL-H	3384	3224	1649	1591	buried, 1270	1007	-	-
Cu(BzySAL-H)	3299, 3439	-	1603	1561	1544, 1250	1009	601	490
Zn(BzySAL-H)	Broad	3227	1597	1576	1541, 1253	1010	590	442
BzySAL-Br	3423	3209	1655	1591	1561, 1268	990	-	-
Cu(BzySAL-Br)	3401, 3529	-	1613	overlap	1558, 1244	995	568	453
Zn(BzySAL-Br)	3422, broad	-	1617	1578	buried, 1253	1007	569	453
BzySAL-Cl	3410	3210	overlap	1592	buried, 1267	1000	-	-
Cu(BzySAL-Cl)	3404, broad	-	1605	overlap	buried, 1245	1001	573	453
Zn(BzySAL-Cl)	3359, broad	-	1615	1581	1558, 1250	1009	559	455

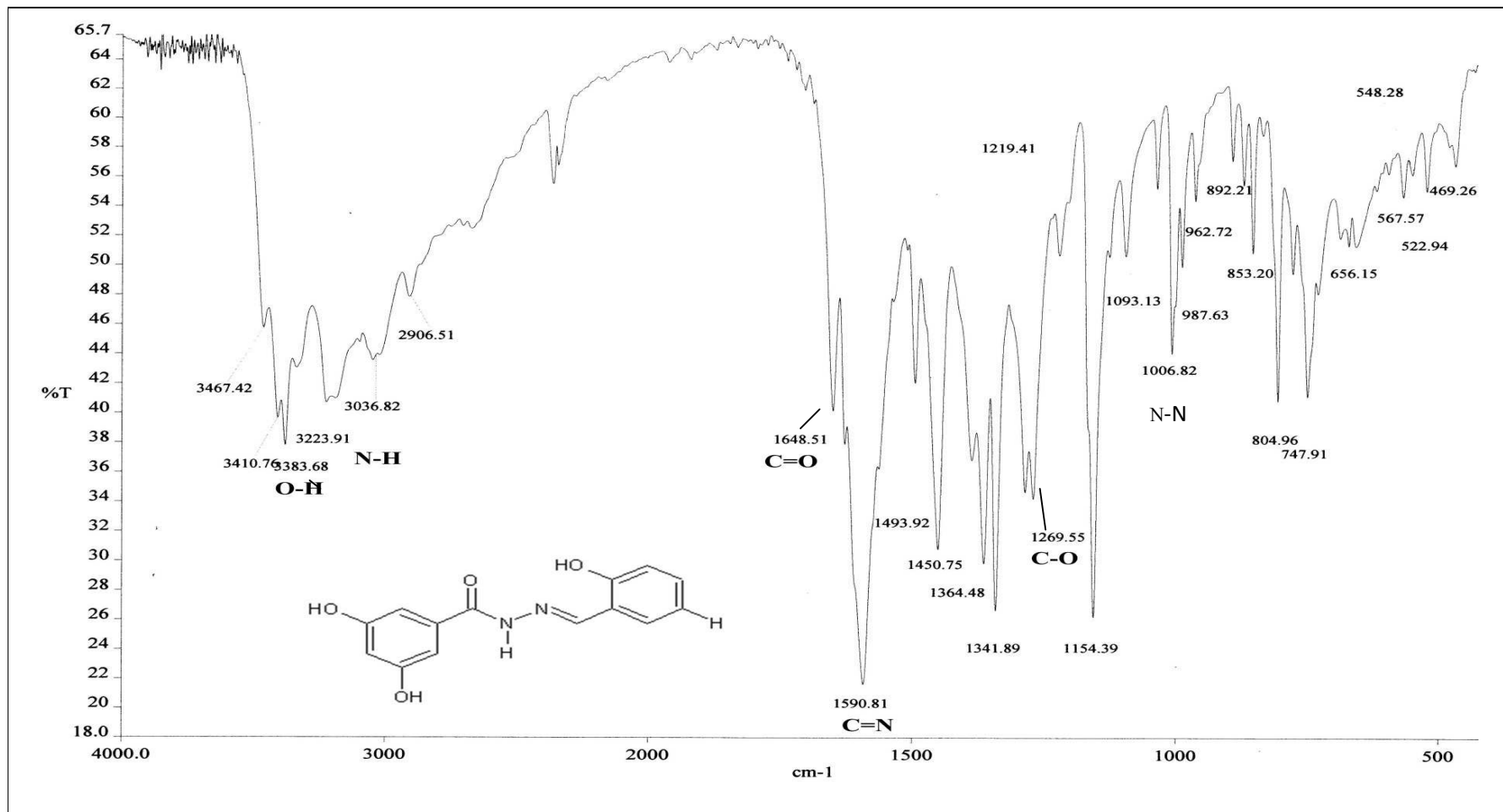


Figure 4.19: IR Spectra of BzySAL-H

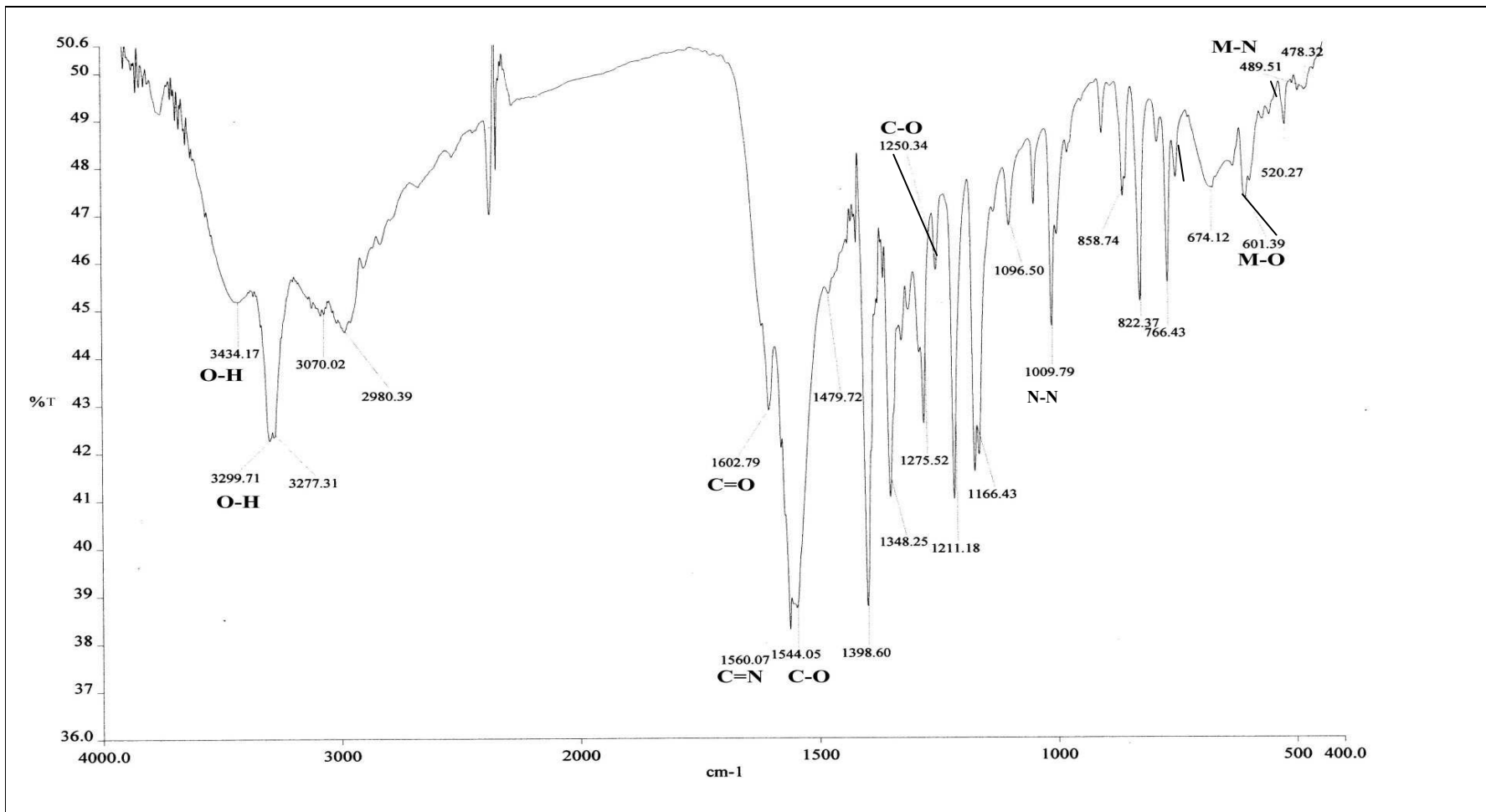


Figure 4.20: IR Spectra of Cu(BzySAL-H)

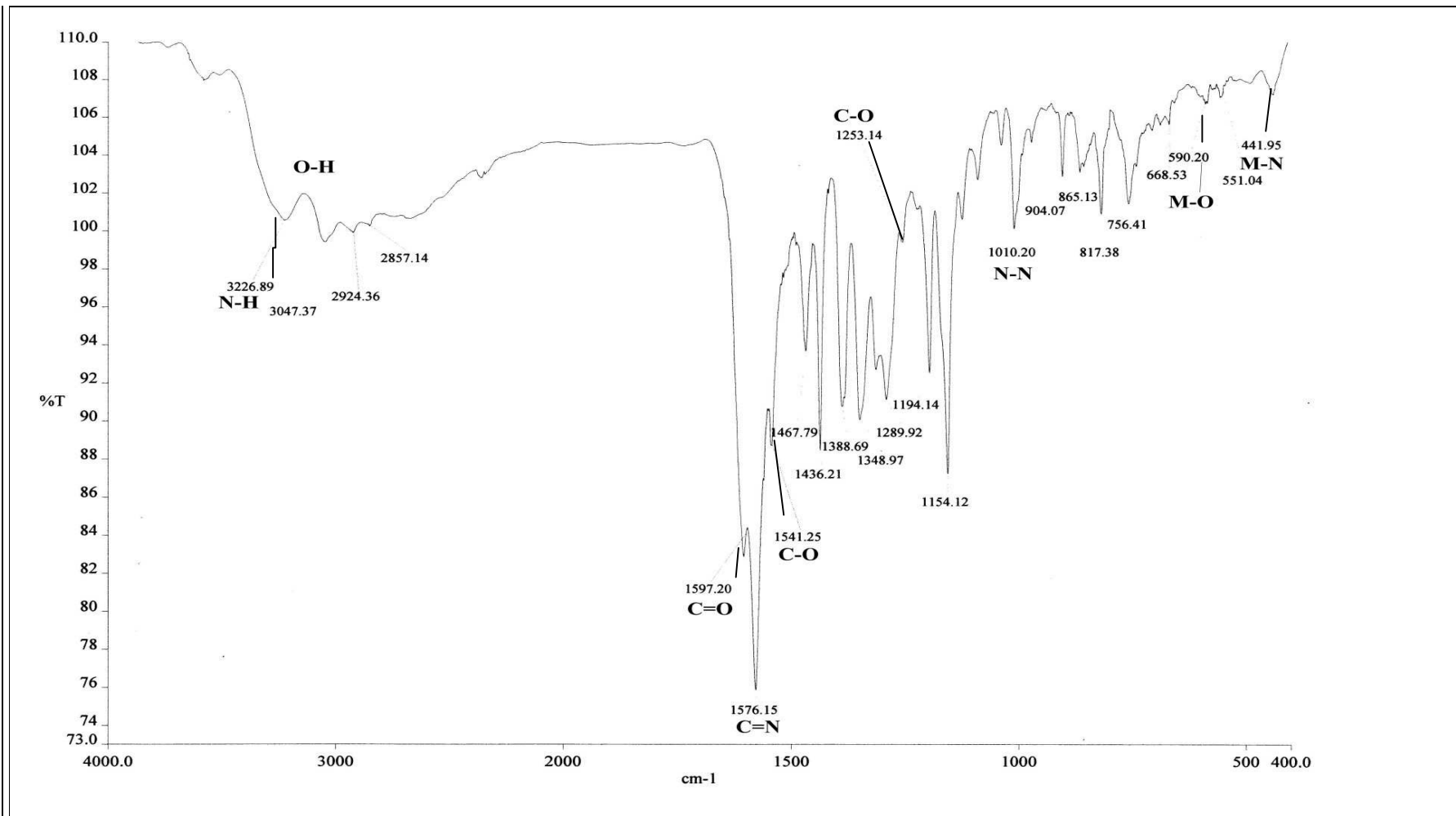


Figure 4.21: IR Spectra of Zn(BzySAL-H)

4.2.2 ¹H NMR Spectral Data

The ¹H NMR spectra of BzySAL series ligands and their Zn(II) complexes are tabulated in table 4.9, following proton numbering as shown in figure 4.23. The spectra are recorded in dimethyl sulphoxide (DMSO) with trimethylsilane (TMS) as internal standard with the chemical shifts expressed in ppm. The spectrum of Cu(II) complexes could not be established as they are expected to be paramagnetic.

All the protons are found at their expected region and the integration values agree with the number of proton obtained from by C, H, N element analyses. The N-H proton (H¹) occupies the greater downfield as singlet which integrated for one proton. This ample evidence proves that the ligand behaves in keto form in solution (Iskander et al., 2000). The hydroxyl proton of the salicylaldehyde moiety (H²) appears at 11.3ppm while the dihydroxyl proton of bezohydrazone moiety (H³) resonates at 9.6ppm with the integration due to two protons. H² resonates at greater downfield compared to H³ due to the inductive effect of the imine group (Pavia et al., 2001). The azomethine (H⁴-C=N) proton of all ligands exhibit a singlet band at 8.5-8.6ppm (Mashaly et al., 2004), and the multiplet peaks of aromatic protons are observed at the range of 6.4-7.6ppm. Thus, the ¹H NMR spectra of the ligands are found to be in good agreement with their proposed structures.

The comparison of the ¹H NMR spectra of the ligands and their Zinc(II) complexes indicates that the ligands act as tridentate ligand that is coordinated to the metal center through the salicylaldehyde oxygen, imine nitrogen and carbonyl oxygen. The absence of proton N-H¹ and O-H² peaks respectively (Gao et al., 1998) indicating the coordination of ligand through deprotonated hydroxyl group and the carbonyl group. The resonances due

to benzohydrazone-OH³ and imine hydrogen (H⁴) experience very slight upfield shifted. The aromatic protons remain unchanged.

Table 4.9: ¹H NMR Spectral Data of BzySAL Series and their Cu(II) and Zn(II) complexes

Compound	Chemical Shift, δ (ppm)				
	H ¹	H ²	H ³	H ⁴	H ^{Ar}
BzySAL-H	11.9	11.3	9.6	8.6	6.4-7.4
Cu(BzySAL-H)	Paramagnetic				
Zn(BzySAL-H)	-	-	9.0	8.6	6.4-7.4
BzySAL-Br	12.0	11.3	9.6	8.5	6.4-7.7
Cu(BzySAL-Br)	Paramagnetic				
Zn(BzySAL-Br)	-	-	9.2	8.5	6.2-7.0
BzySAL-Cl	12.0	11.3	9.6	8.5	6.4-7.6
Cu(BzySAL-Cl)	Paramagnetic				
Zn(BzySAL-Cl)	-	-	9.2	8.5	6.2-7.0

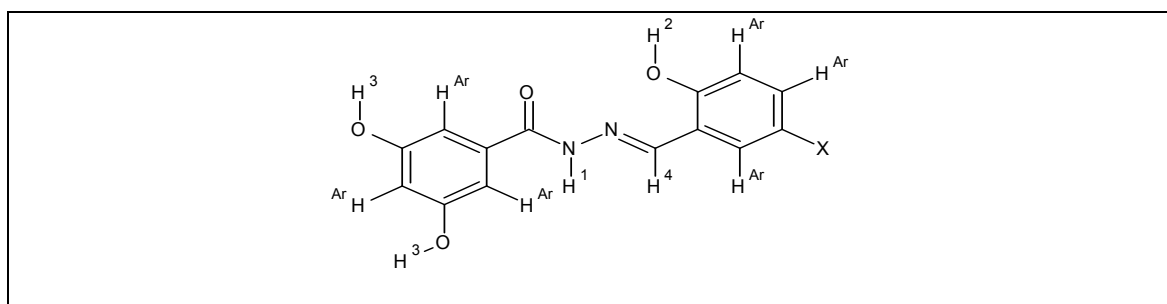


Figure 4.22: Proton numbering scheme of BzySAL Series ligand

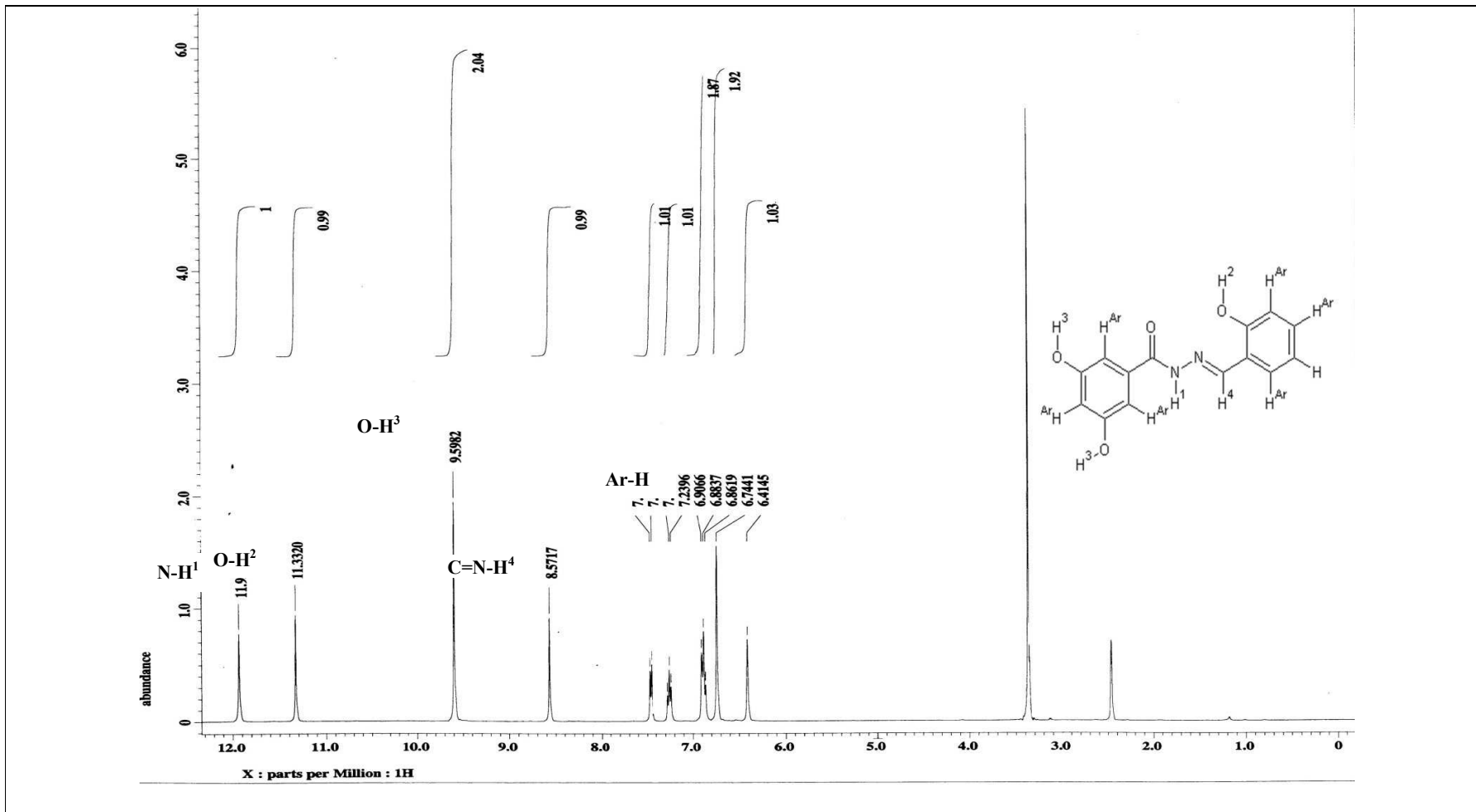


Figure 4.23: ¹H NMR Spectra of BzySAL-H

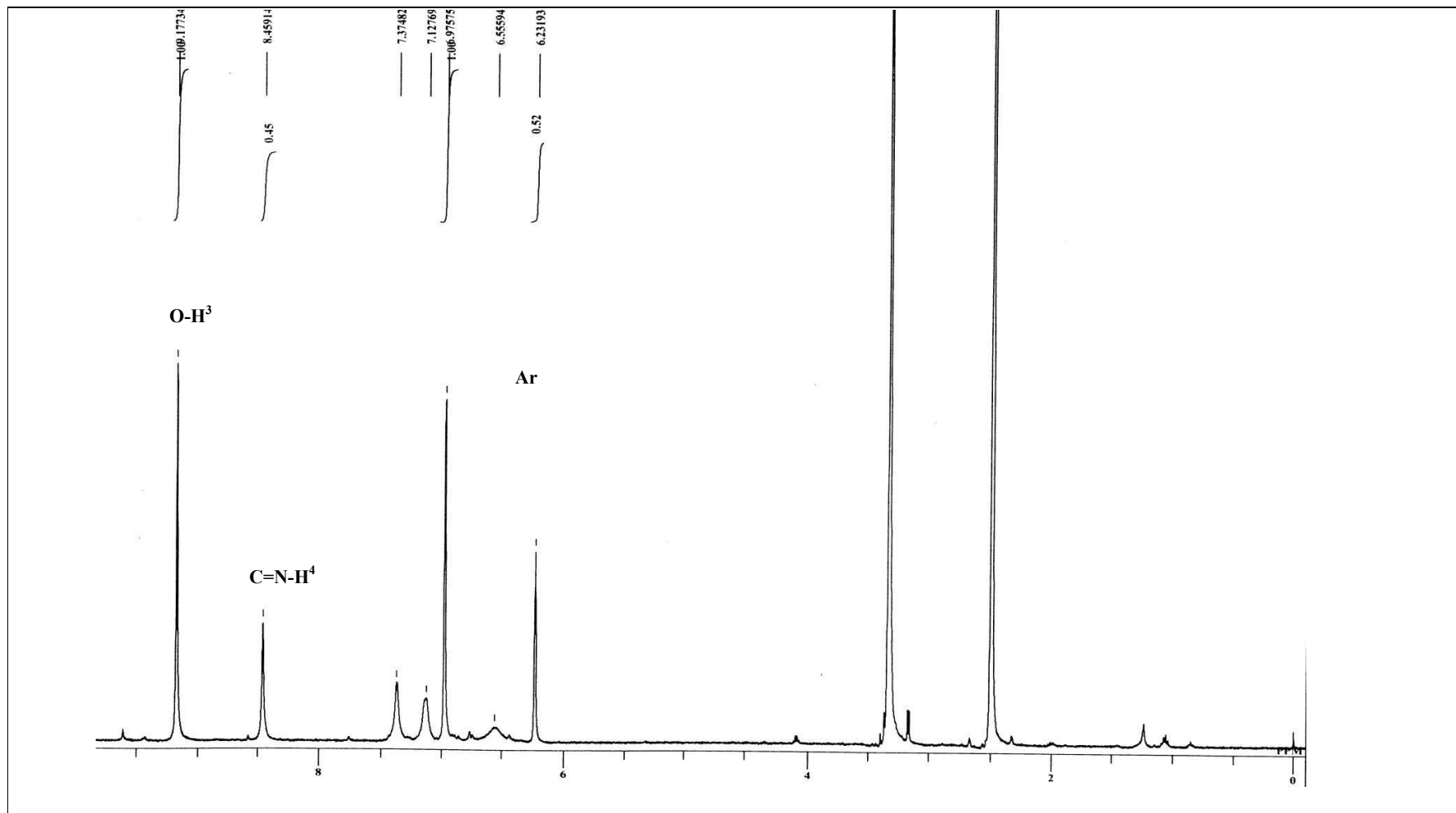


Figure 4.24: ^1H NMR Spectra of Zn(BzySAL-H)

4.2.3 ^{13}C NMR Spectral Data

The ^{13}C NMR spectra of the ligands are summarized and depicted in table 4.10. The carbon numbering scheme is shown in figure 4.25.

The most downfield peak appears at 163.5-163.7ppm is assigned to the $\text{C}^1=\text{O}$ and the deshielding is due to the electronegative effect of the oxygen directly attached to the carbon (Pavia et al., 2009). The hydroxyl- C^2 of benzohydrazone and C^3 of salicylaldehyde moieties resonate at 158.9-159.0ppm and 156.9-158.0ppm respectively. The bands of aromatic carbons exhibit at the range 106.3-135.3ppm while the azomethine $\text{C}^4=\text{N}$ peak is observed at 146.2-148.8ppm. The assignment of the ^{13}C NMR spectra is found to be in a good agreement with their respective proposed structures.

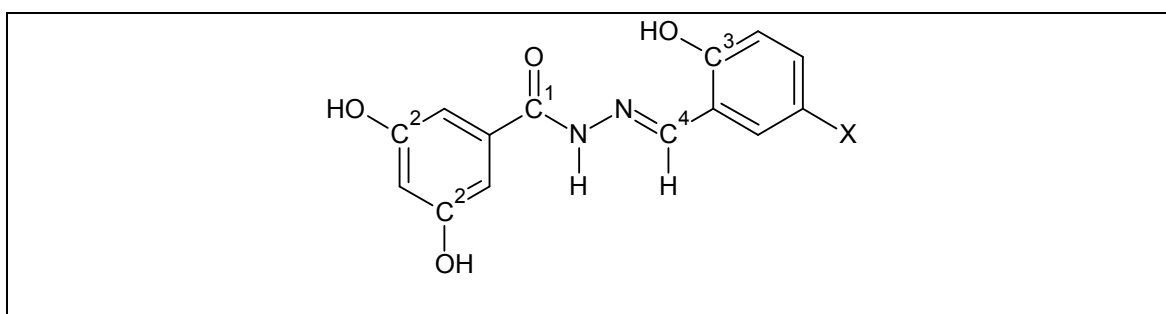


Figure 4.25: Carbon numbering scheme of BzySAL Series Ligands

Table 4.10: ^{13}C NMR Spectral Data of BzySAL Series

Compound	Chemical Shift (ppm)				
	C ₁ =O	C ₂ -OH	C ₃ -OH	C ₄ =N	C-Ar
BzySAL-H	163.5	159.0	158.0	148.8	106.3-135.3
BzySAL-Br	163.7	158.9	156.9	146.2	106.4-135.2
BzySAL-Cl	163.7	158.9	156.9	146.2	106.4-135.2

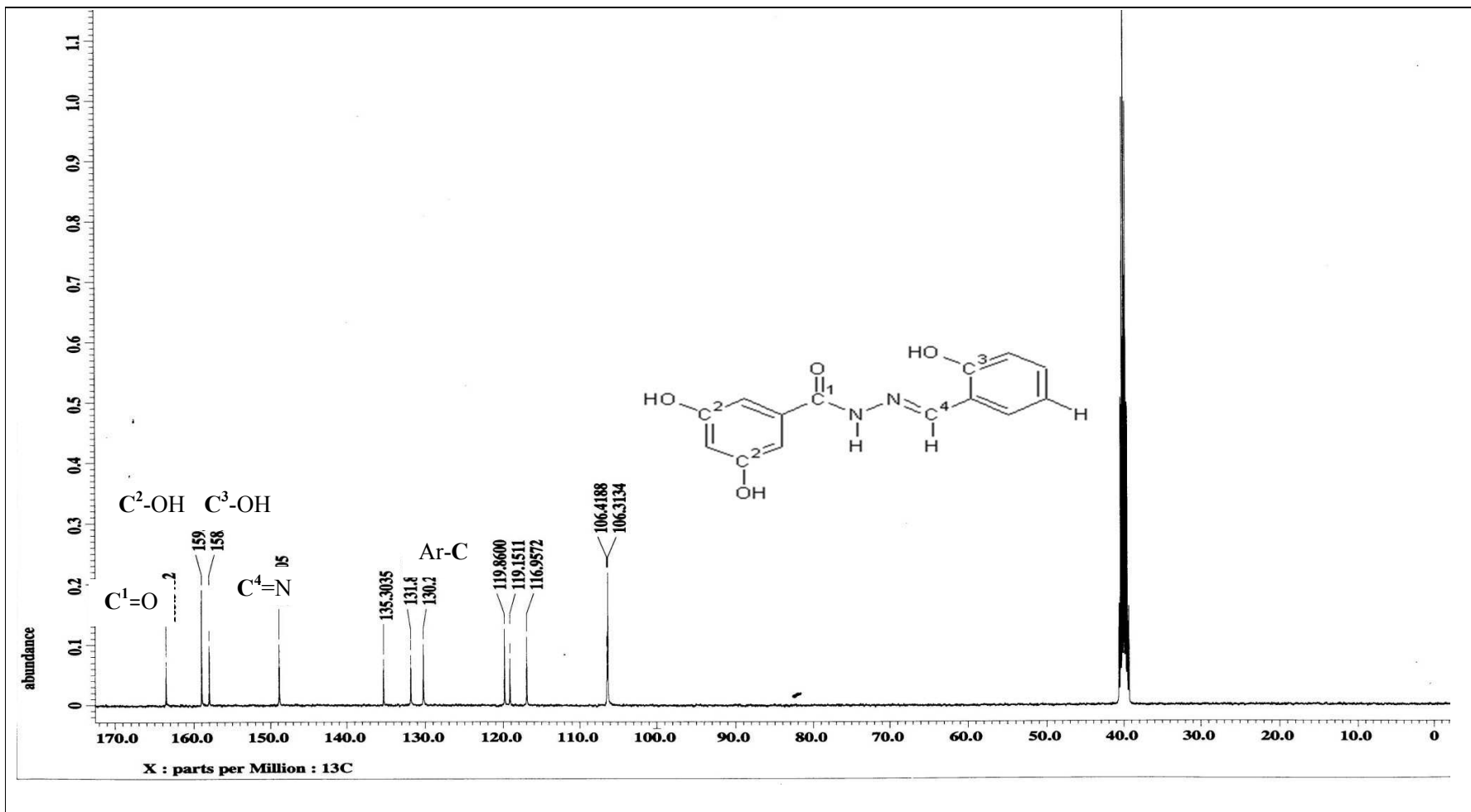


Figure 4.26: ^{13}C NMR Spectral of BzySAL-H

4.2.4 UV-Vis Spectral Data

The electronic absorption spectrum of the ligands and their Cu(II) and Zn(II) complexes were recorded at 200-800nm in dimethyl sulphoxide (DMSO) and are depicted in table 4.11.

The spectrum of free ligand is expected to exhibit two important characteristic bands represent the $\pi \rightarrow \pi^*$ transition of aromatic rings and $n \rightarrow \pi^*$ transition of azomethine (-NH-N=C-) group (Nath et al., 1991). The appearance of new intense (LMCT) band, and the red shift of the $\pi \rightarrow \pi^*$ transition and $n \rightarrow \pi^*$ transition bands to lower frequency (Zhu et al., 1996) indicate the formation of metal complexes. The Cu(II) complexes, on the other hand, will exhibit a broad band correspond to the d-d transition.

The spectrum of free ligand shows a shoulder band at 291-299nm attributable to $n \rightarrow \pi^*$ transition of azomethine group while the intense band at 329-340nm is assigned to the $\pi \rightarrow \pi^*$ transition of aromatic rings (Mala et al., 1995).

The formation of the Cu(II) complexes is indicated by the shifting of $n \rightarrow \pi^*$ and $\pi \rightarrow \pi^*$ transition band to higher energy (bathochromical shift). The appearance of charge transfers (LMCT) band at 397-398nm due to the transition of the lone pairs of phenolic oxygen donor to metal ion (Ainscough et al., 1998) further support the coordination of the ligand to the metal. The exhibition of a low intensity broad band around 653-692nm is assigned to d-d transition. The d-d transition of Cu(BzySAL-H) appears at 692nm indicates that it employs square pyramidal geometry (Lever, 1984) while Cu(BzySAL-Br) and Cu(BzySAL-Cl) are proposed to have square planar geometry (Ran et al., 2011, Arish et al., 2010).

In the Zn(II) complexes, both of $\pi \rightarrow \pi^*$ and $n \rightarrow \pi^*$ transition bands experience red shift to the lower frequencies of 226-265nm and 305-309nm respectively. The formation of the Zn(II) complexes are further supported by the exhibition of a new band centered at 363-398nm associated with the charge transfer between the lone pair of phenolate oxygen and metal ion. As expected, d-d transitions do not exist for d^{10} system of Zn(II) complexes.

Table 4.11: UV-Vis Spectral Data of BzySAL Series and their Cu(II) and Zn(II) complexes

Compound	Wavelength (nm)			
	$\pi \rightarrow \pi^*$	$n \rightarrow \pi^*$	LMCT	d-d
BzySAL-H	299	329	-	-
Cu(BzySAL-H)	226	297	397	692
Zn(BzySAL-H)	262	305	363	-
BzySAL-Br	293	340	-	-
Cu(BzySAL-Br)	233	313	398	653
Zn(BzySAL-Br)	262	309	397	-
BzySAL-Cl	291	339	-	-
Cu(BzySAL-Cl)	232	313	397	654
Zn(BzySAL-Cl)	265	308	398	-

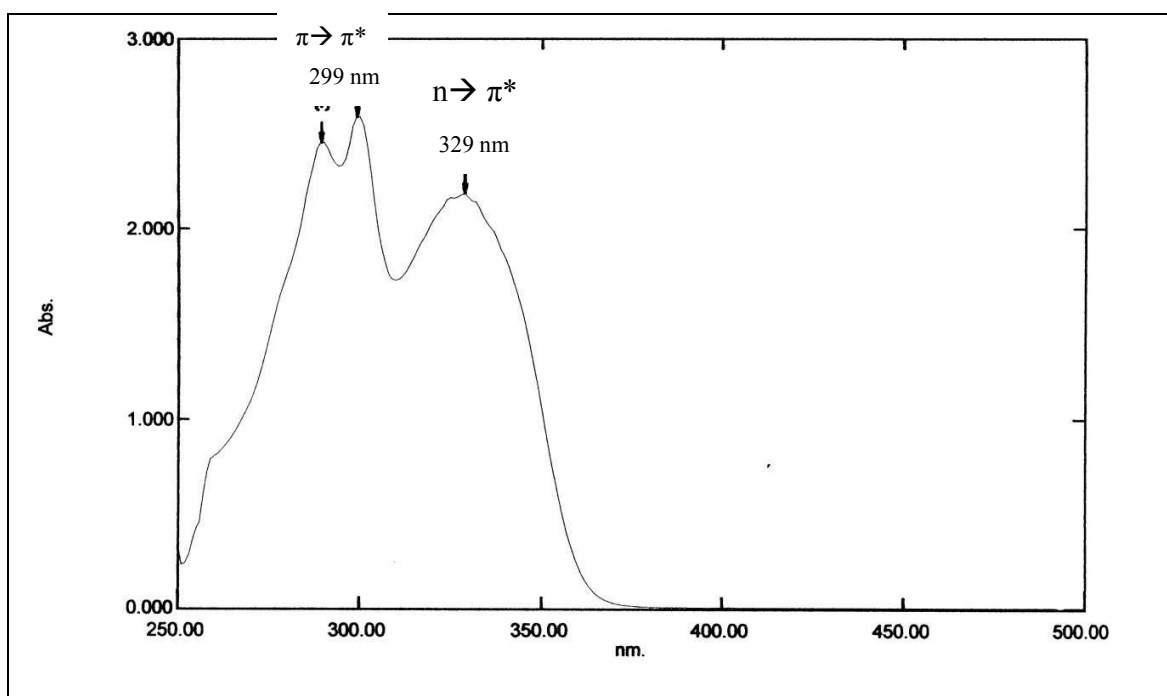


Figure 4.27: UV Spectra of BzySAL-H

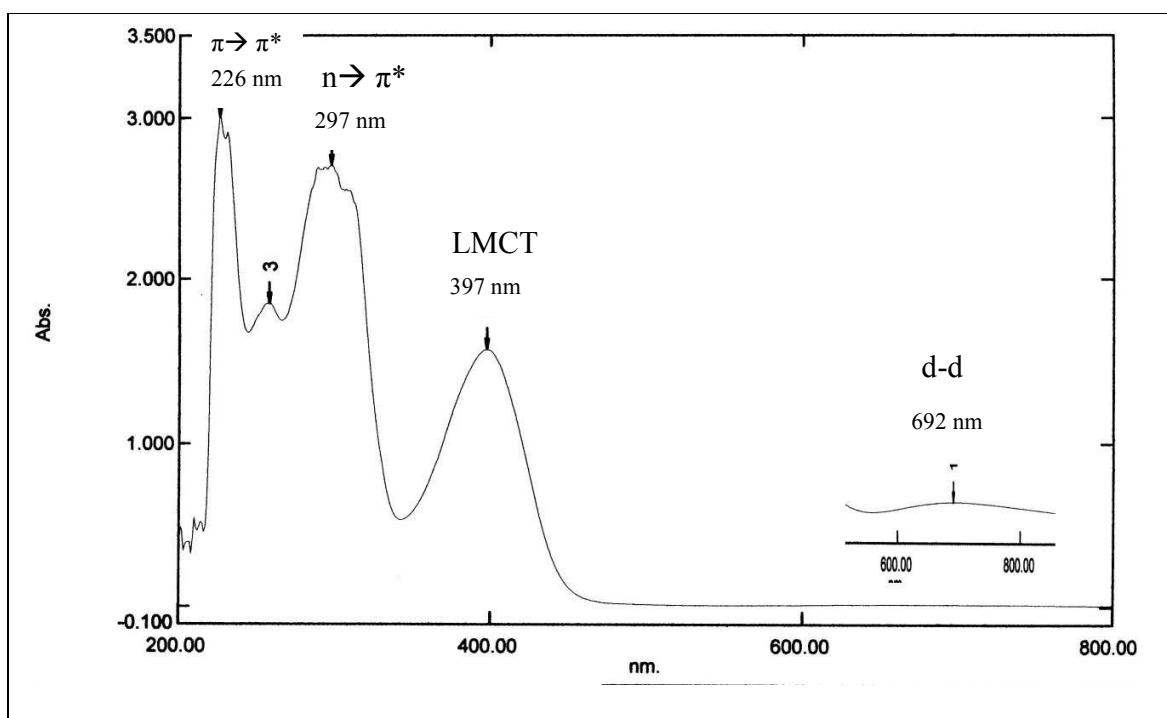


Figure 4.28 UV Spectra of Cu(BzySAL-H)

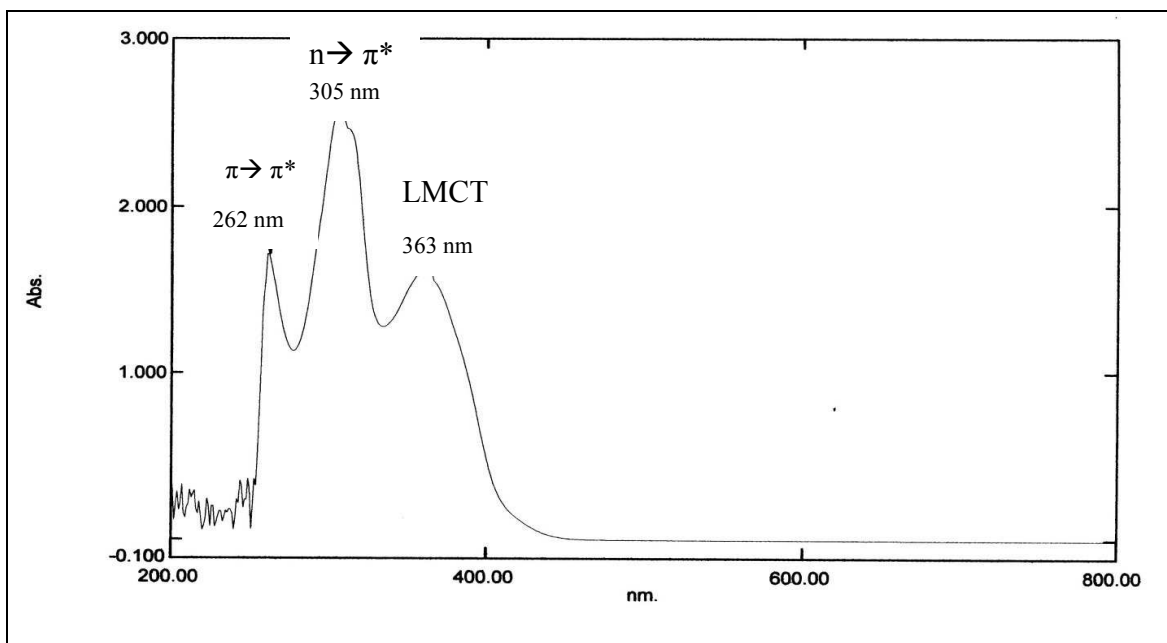


Figure 4.29: UV Spectra of Zn(BzySAL-H)

4.2.5 Metal analysis by Atomic Absorption Spectroscopy (AAS)

Acid digestion method ASTM3005 (American Society for Testing Material) with some modification was employed to analyse the metal composition of complexes.

Firstly, the sample was weighted accurately before the addition of 2ml of concentrated nitric acid followed by 5ml of concentrated hydrochloric acid. The mixture was then heated on the hot plate until the solution became clear. The solution was allowed to cool, and adjusted to final volume 100ml with distilled water. The sample was replicated by diluting 0.5ml of stock solution to the final volume of 25ml. The experimental composition of the metal was calculated as follows:

$$\text{Experimental metal composition (\%)} = (\text{concentration (ppm)} \times 0.25) / \text{mass used}$$

The experimental metal composition and the theoretical percentage of the proposed structures show a good agreement indicating the formation of the desired complexes.

Table 4.12: Experimental and Theoretical Metal Composition of the Zn(II) complexes

Compound	Mass used(g)	Concentration (mg/L)	Experimental metal composition	Theoretical metal composition
Cu(BzySAL-H)	0.0047	0.168	17.87	17.14
Zn(BzySAL-H)	0.0200	0.441	11.03	10.76
Cu(BzySAL-Br)	0.0200	0.594	14.85	15.36
Zn(BzySAL-Br)	0.0070	0.190	13.57	15.78
Cu(BzySAL-Cl)	0.0150	0.520	14.85	15.30
Zn(BzySAL-Cl)	0.0170	0.451	15.03	16.85

4.2.6 X-ray Crystallographic Analyses of Schiff Base

Ligand of BzySAL-Br

Only yellow crystal of BzySAL-Br was obtained and subjected to x-ray crystallography analysis. The crystal data and structure refinement are tabulated in table 4.13 and the thermal ellipsoid plot is depicted in figure 4.31 while the packing view of the compound is shown in figure 4.32.

In the analysis, the crystal structure of the compound $C_{14}H_{11}BrN_2O_4$ is found to be almost planar with an r.m.s. deviation for the non-H atom of 0.16Å. The Schiff base molecules and the water molecules are linked together by the intermolecular N-H \cdots O and O-H \cdots O hydrogen bonds, leading to layers parallel to the *bc* plane. An intramolecular O-H \cdots N hydrogen bond involving the imine N atom and a hydroxyl substituent is also observed (Saharin et al., 2010).

As represented in the packing diagram (figure 4.32), the molecules are bound together via intramolecular and intermolecular hydrogen bond. The intermolecular N-H \cdots O formation between two independent molecules in asymmetric units creates a one-dimensional zigzag infinite layer structure.

The carbon-bound H atoms are placed in calculated positions (C-H fixed to 0.93Å) and treated as riding on their parent carbon atoms with $U_{iso}(H)$ set to $1.2U_{eq}(\text{carrier C})$. The nitrogen- and oxygen-bound H atoms are located in a difference map and refined as free atoms, with N-H and O-H distances restrained to 0.86(2) and 0.82(2)Å, respectively. The hydrogen bond geometry is depicted in table 4.14.

Table 4.13: Crystal data and structure refinement of BzySAL-Br

Empirical formula	C ₁₄ H ₁₁ BrN ₂ O ₄ ·H ₂ O
Formula weight	369.17
Temperature (K)	296 K
Crystal size (mm)	0.58 × 0.33 × 0.06 mm
Colour	Yellow
Wavelength (Å)	0.71073 Å
Crystal system	Monoclinic
Space group	P21/c
Unit cell dimension	a (Å) = 13.5685(3) α (°) = 90 b (Å) = 8.0532(2) β (°) = 100.186(1) c (Å) = 13.2447(2) γ (°) = 90
Volume (Å ³)	1424.44(5)
Calculated density, Z	4
Absorption coefficient, μ	2.91 mm ⁻¹
F(000)	744
Theta range for data collection (°)	3.0–26.1
Index ranges	-16 ≤ h ≤ 16; -9 ≤ k ≤ 9; -15 ≤ l ≤ 15
Reflection collected	9148
Independent reflection	2579
R(int)	0.034
Data/restraint/parameter	2579/6/217
Absorption correction	multi-scan
Goodness-of-fit on F ²	1.04
Final R indices [I > 2σ(I)]	R1 = 0.031, wR2 = 0.077
Largest diff. peak and hole (e Å ⁻³)	0.45 and -0.56

Table 4.14: Hydrogen-bond geometry (Å, °)

<i>D</i> —H... <i>A</i>	<i>D</i> —H	H... <i>A</i>	<i>D</i> ... <i>A</i>	<i>D</i> —H... <i>A</i>
O1—H1...N1	0.81 (2)	1.95 (2)	2.657 (2)	145 (3)
N2—H2N...O2	0.85 (2)	2.07 (2)	2.913 (3)	170 (2)
O11—H11...O8ⁱ	0.83 (2)	1.94 (2)	2.750 (2)	168 (3)
O13—H13...O1ⁱⁱ	0.79 (2)	2.19 (2)	2.959 (2)	165 (3)
O2—H2A...O8ⁱ	0.81 (2)	1.98 (2)	2.776 (3)	171 (4)
O2—H2B...O11ⁱⁱⁱ	0.83 (2)	2.06 (2)	2.861 (3)	165 (3)

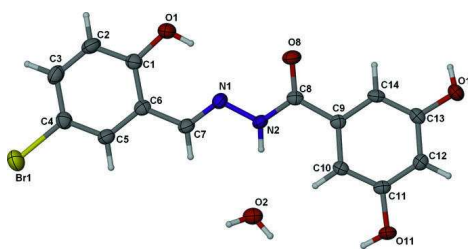


Figure 4.30: Thermal ellipsoids plot of BzySAL-Br. Displacement ellipsoids are drawn at the 50% probability level, and H atom is shown as spheres of arbitrary radii.

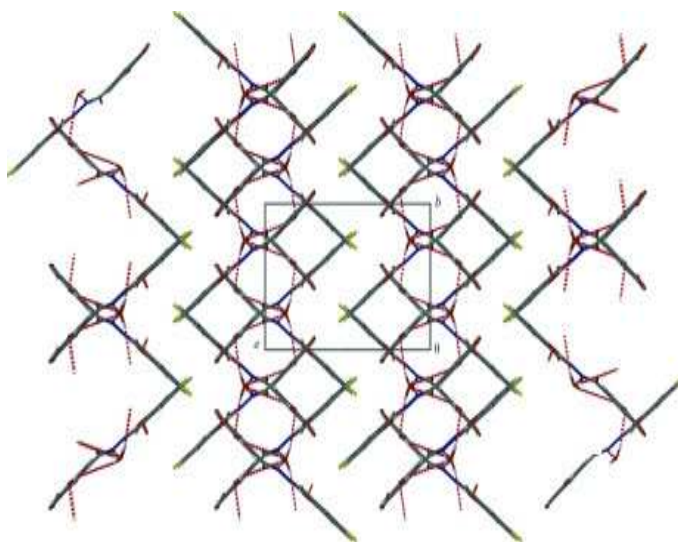


Figure 4.31: Packing view looking down the crystallographic b unit cell edge.

4.2.7 Proposed Structures of BzySAL Series and their Zn(II) complexes

The spectroscopic and elemental analyses of the compounds make a good agreement with the proposed structural formula of the ligands.

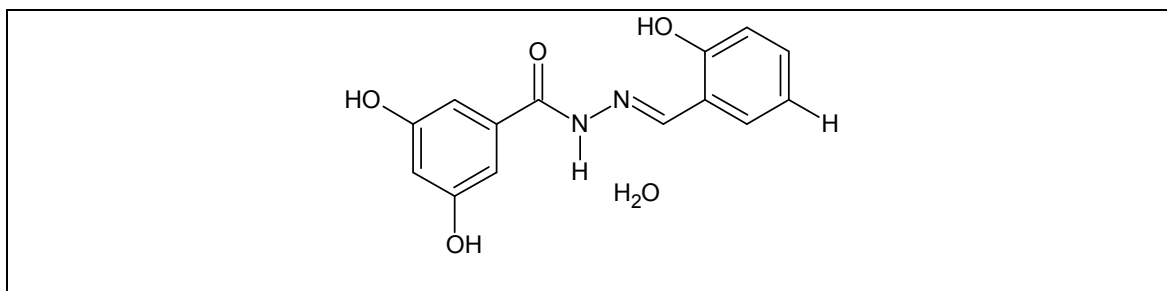


Figure 4.32: Proposed structure of BzySAL-H

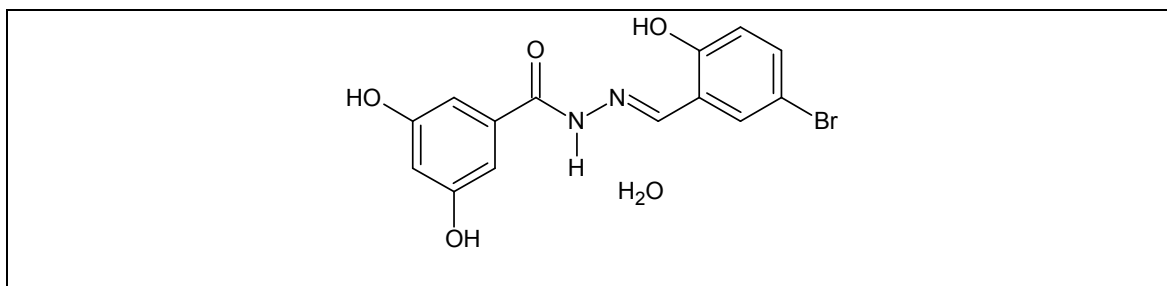


Figure 4.33: Proposed structure of BzySAL-Br

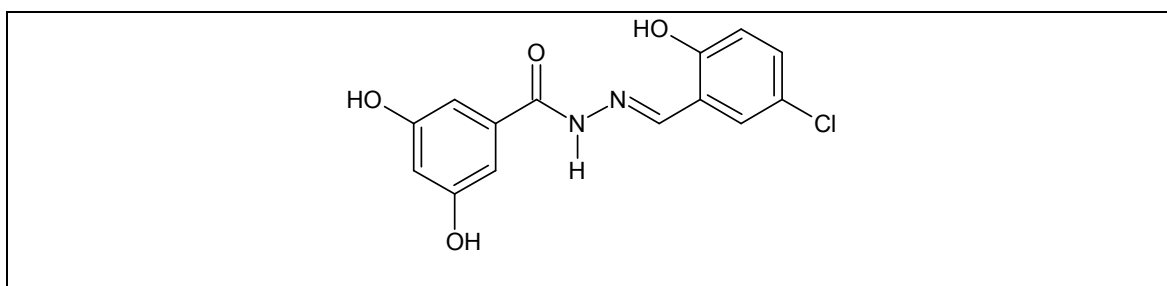


Figure 4.34: Proposed structure of BzySAL-Cl

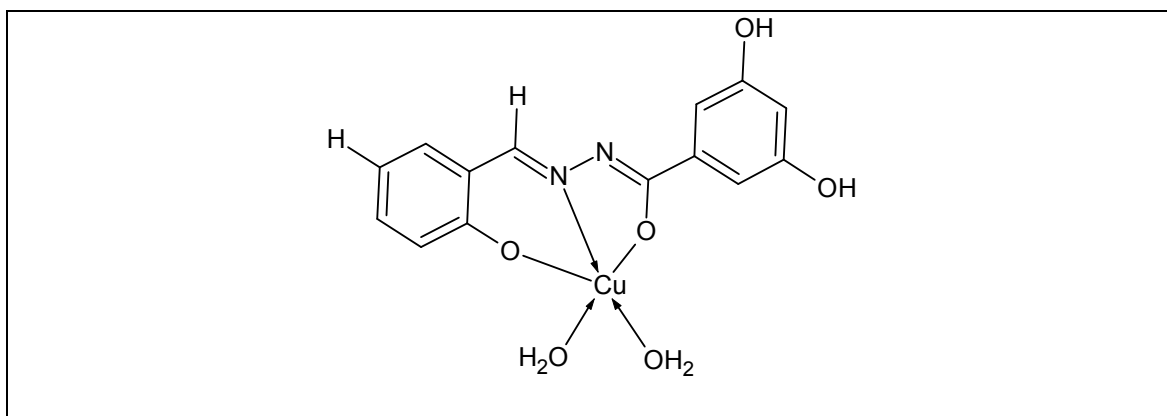


Figure 4.35: Proposed structure of Cu(BzySAL-H)

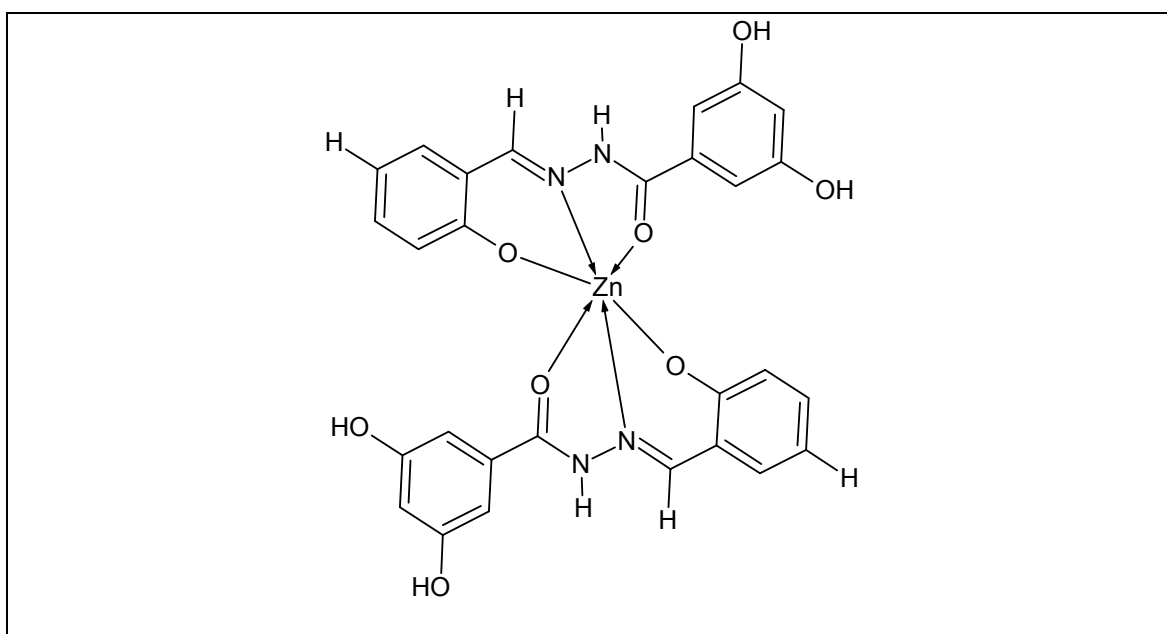


Figure 4.36: Proposed structure of Zn(BzySAL-H)

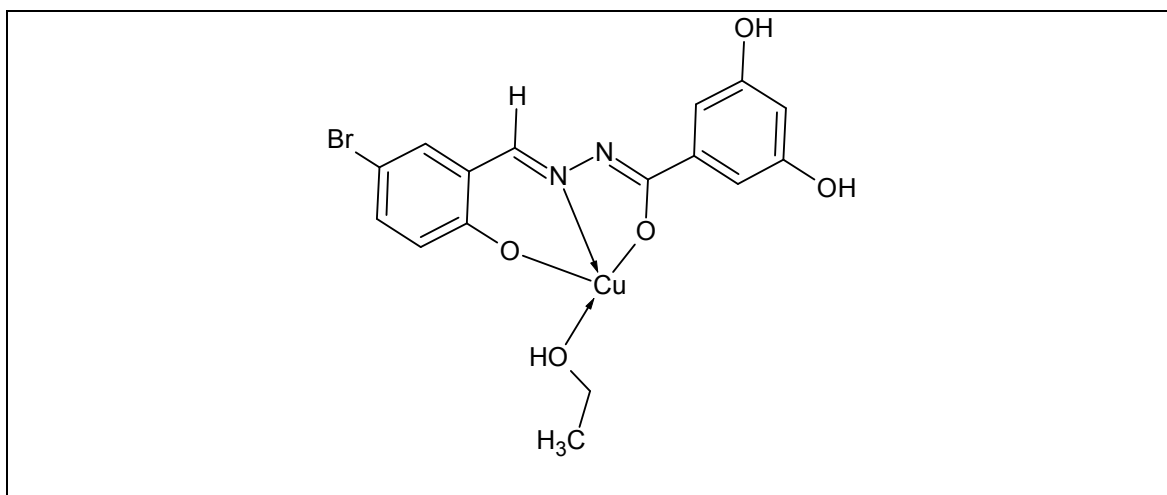


Figure 4.37: Proposed structure of Cu(BzySAL-Br)

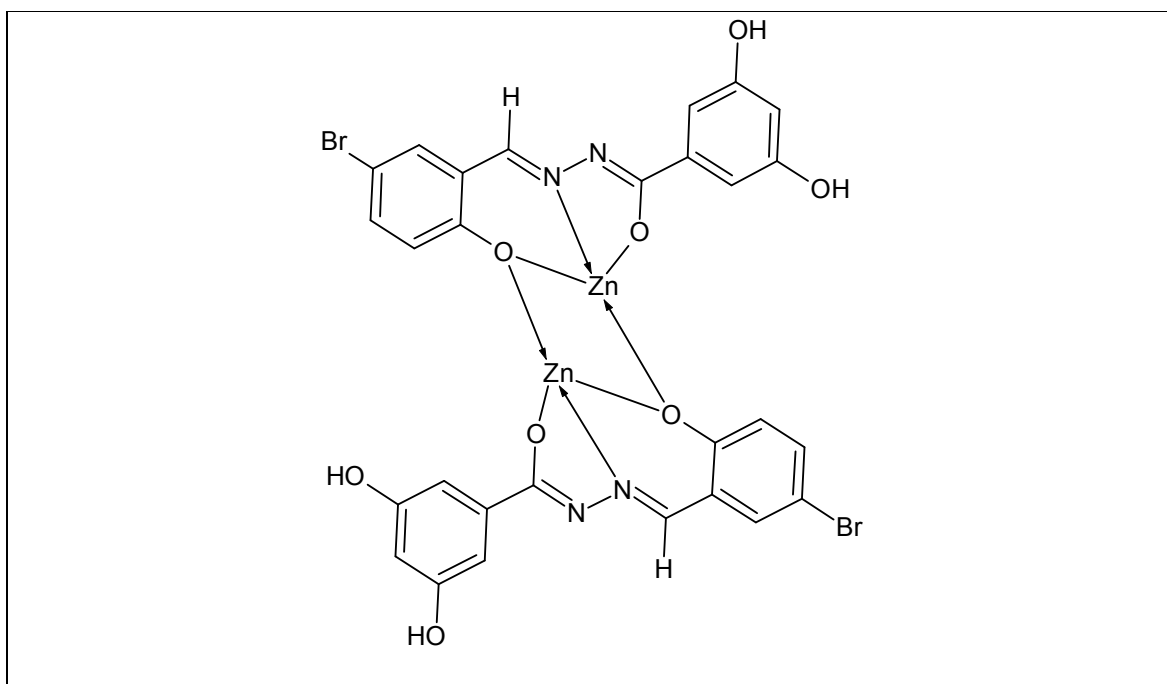


Figure 4.38: Proposed structure of Zn(BzySAL-Br)

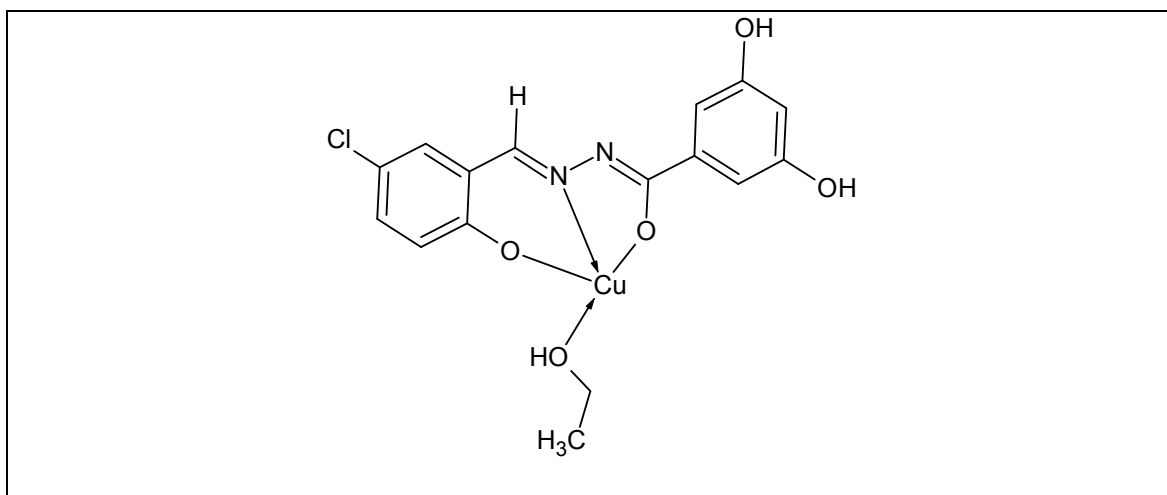


Figure 4.39: Proposed structure of Cu(BzySAL-Cl)

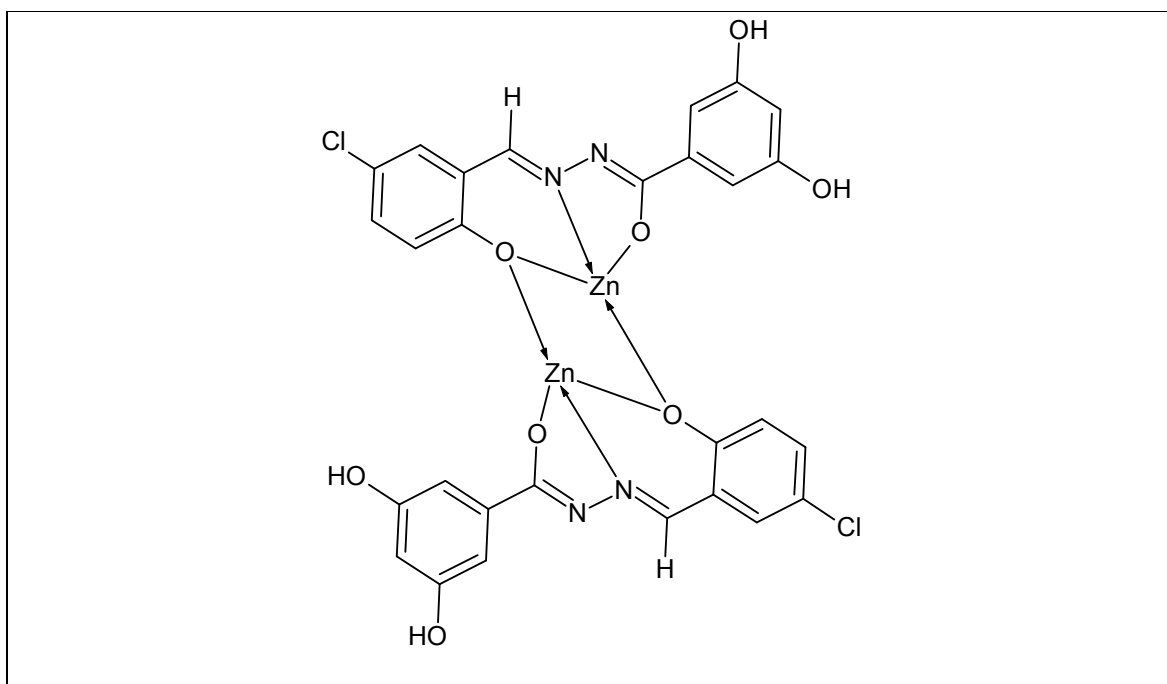


Figure 4.40: Proposed structure of Zn(BzySAL-Cl)

4.3 Cytotoxicity

4.3.1 Cytotoxicity of BzyHAP and BzySAL series Compounds.

The results of cytotoxicity activity of all synthesized compounds are represented in table 4.15. The compounds have been tested against normal cell line (WRL-68), prostate cancer cell line (PC-3), colon cancer cell line (HT-29), and lung cancer cell line (A549). The potency of cell growth inhibition for each compound is expressed as an EC₅₀ value, defined as the concentration that caused a 50% loss of cell growth.

Table 4.15: Cytotoxicity of ligands and their metal complexes on normal cell lines and several cancer cell lines (EC₅₀ µg/ml).

Compound	WRL-68	PC-3	HT-29	A549
BzyHAP-H	>50	>50	>50	>50
BzyHAP-Br	>50	>50	>50	>50
BzyHAP-Cl	>50	>50	>50	>50
BzySAL-H	>50	>50	>50	>50
BzySAL-Br	>50	>50	>50	>50
BzySAL-Cl	>50	>50	>50	>50
Cu(BzySAL-H)	18.9	>50	13.5	24.3
Cu(BzySAL-Br)	21.6	>50	17.9	31.4
Cu(BzySAL-Cl)	18.2	>50	14.3	27.4
Zn(BzyHAP-H)	>50	>50	>50	>50
Zn(BzyHAP-Br)	>50	>50	>50	>50
Zn(BzyHAP-Cl)	>50	>50	>50	>50
Zn(BzySAL-H)	>50	>50	>50	>50
Zn(BzySAL-Br)	>50	>50	>50	>50
Zn(BzySAL-Cl)	>50	>50	>50	>50

In general, all ligands and their Zinc(II) complexes exhibit high value of EC_{50} and are considered as inactive. Only Cu(II) complexes show moderate growth inhibition towards normal cell line WRL-68 and cancerous cell line HT-29 and A549. In contrast, they are inactive against prostate cancer cell line PC-3. It can be concluded that the coordination of the ligand to Cu(II) ion increases the growth inhibition potential of the ligand.

4.4. Antioxidant Activity

The antioxidants play key role in minimizing harmful effects of oxidative stress. In general, various metabolic processes generate different reactive free radicals, mainly reactive oxygen species (ROS). The increasing level of ROS in systemic level can damage the structure of biomolecules and alter their functionality thus leading to cellular dysfunction and cell death. It can be related to the health problems such as cancer, age-related disease and cardiovascular diseases (Mishra et al, 2011). 2,2-diphenylpicrylhydrazyl (DPPH) assay and ferric reducing antioxidant power (FRAP) assay are the basis of common antioxidant assays and are routinely practiced for the assessment of antiradical properties of different compounds.

DPPH assay is considered as one of the standard and easy calorimetric method for antioxidant properties evaluation. DPPH is a stable radical in solution, appears as purple which absorbed at 515nm in methanol. DPPH will accept a hydrogen atom from the antioxidant (scavenger molecule) and reduced to DPPH₂ employing yellow colour with concomitant decrease in absorbance (Blois, 1958). FRAP assay is an accurate method to assess anti-oxidant 'power'. At low pH, reduction of ferric tripyridyl triazine complex to ferrous form can be monitored by measuring the change in absorbance at 593nm. FRAP

assay is non-specific, inexpensive method with straightforward procedure that offers highly reproducible results. Lower FRAP values indicate the lower production of reactive oxygen species (ROS) or could be the response to an increase of ROS that react with antioxidants (Griffin et al., 2004).

4.4.1 DPPH Scavenging Activity of Ligands and complexes of BzyHAP series

The compounds were subjected to DPPH scavenging capacities test at 20 $\mu\text{g/mL}$ and 100 $\mu\text{g/mL}$ with vitamin C as the standard. The results obtained are expressed in percentage (%) of inhibition and are tabulated in the bar chart (Figure 4.41). Generally, all compounds show significantly moderate DPPH inhibition compared to the standard vitamin C. The highest DPPH inhibition percentage is recorded by the unsubstituted BzyHAP-H ligand whereas BzyHAP-Cl shows the lowest inhibition. The coordination to Zn(II) ion reduces the inhibition ability of BzyHAP-H and BzyHAP-Br. In contrary, Zn(BzyHAP-Cl) shows highest activity among the complexes.

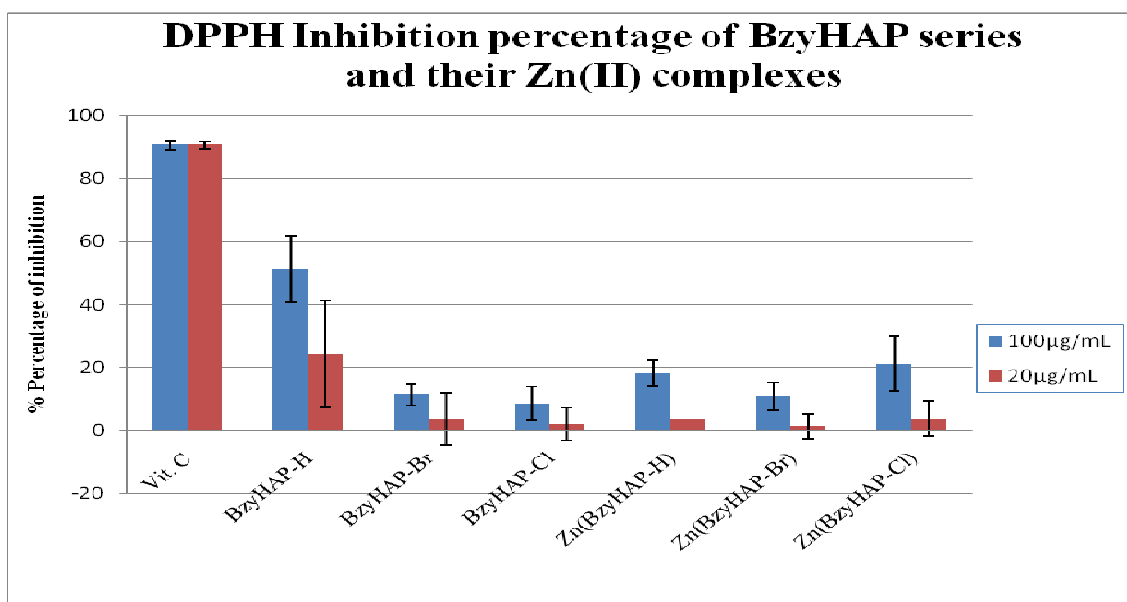


Figure 4.41: DPPH inhibition percentage of BzyHAP series and their Zn(II) complexes

4.4.2 FRAP Value of Ligands and complexes of BzyHAP series

The ferric reducing anti-oxidant power (FRAP) of the compound measured in comparison with vitamin C as the standard. The results obtained are expressed in μM ferrous equivalents and are tabulated in the bar chart (Figure 4.42). Although the reducing ability of the studied compounds is comparable to the standard, none of them show higher activity than it. All of the compounds tested reduce the ferric TPTZ complex used in the FRAP assay less than the standard vitamin C. BzyHAP-H displays the highest ferric reducing efficiency while Br-substituted ligand is the lowest among the ligands. Meanwhile, the complexation of BzyHAP-H and BzyHAP-Cl has led to the decreasing of the FRAP value. On the other hand, the Zn(BzyHAP-Br) shows a slight increase in the reducing power.

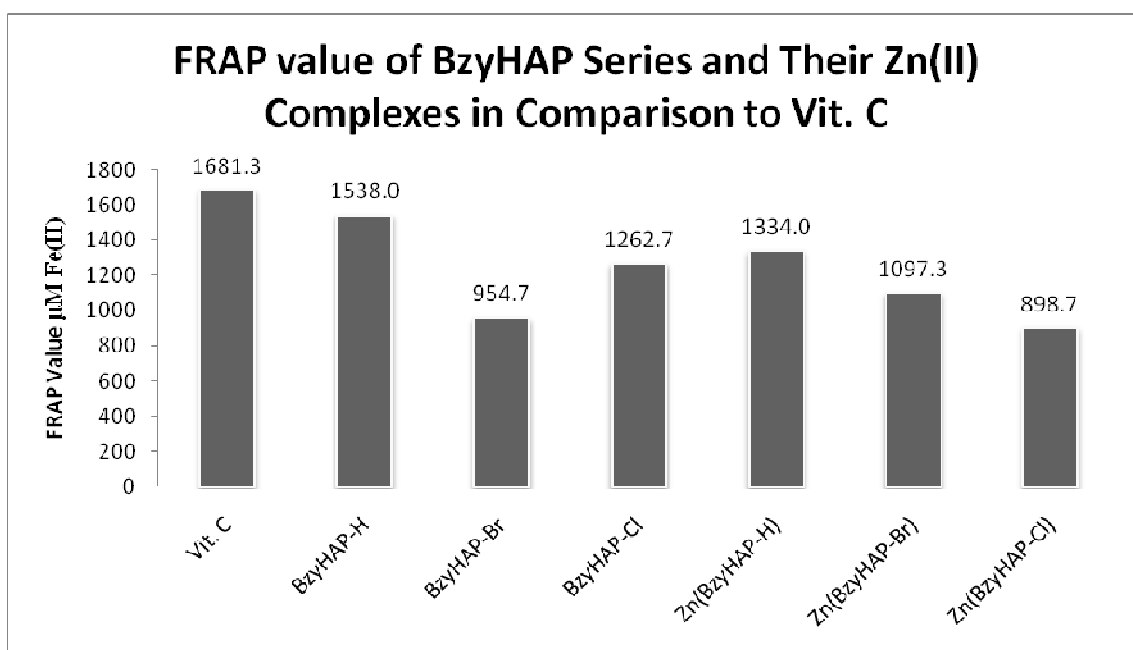


Figure 4.42: FRAP value of BzyHAP series and their Zn(II) complexes

4.4.3 DPPH Scavenging Activity of Ligands and complexes of BzySAL series

The compounds were subjected to DPPH scavenging capacities test at 20 μ g/mL and 100 μ g/mL with vitamin C as the standard. The results obtained are expressed in percentage (%) of inhibition and are tabulated in the bar chart (Figure 4.3). In general, all compounds of the series displayed relatively low DPPH inhibition percentage. None of them having potential to suppress DPPH radicals compared to vitamin C. The highest DPPH inhibition percentage is recorded by the Zn(BzySAL-Br) ligand whereas the ligand BzySAL-Cl shows the lowest inhibition. The coordination to metal(II) ion slightly increases the inhibition ability of the ligands.

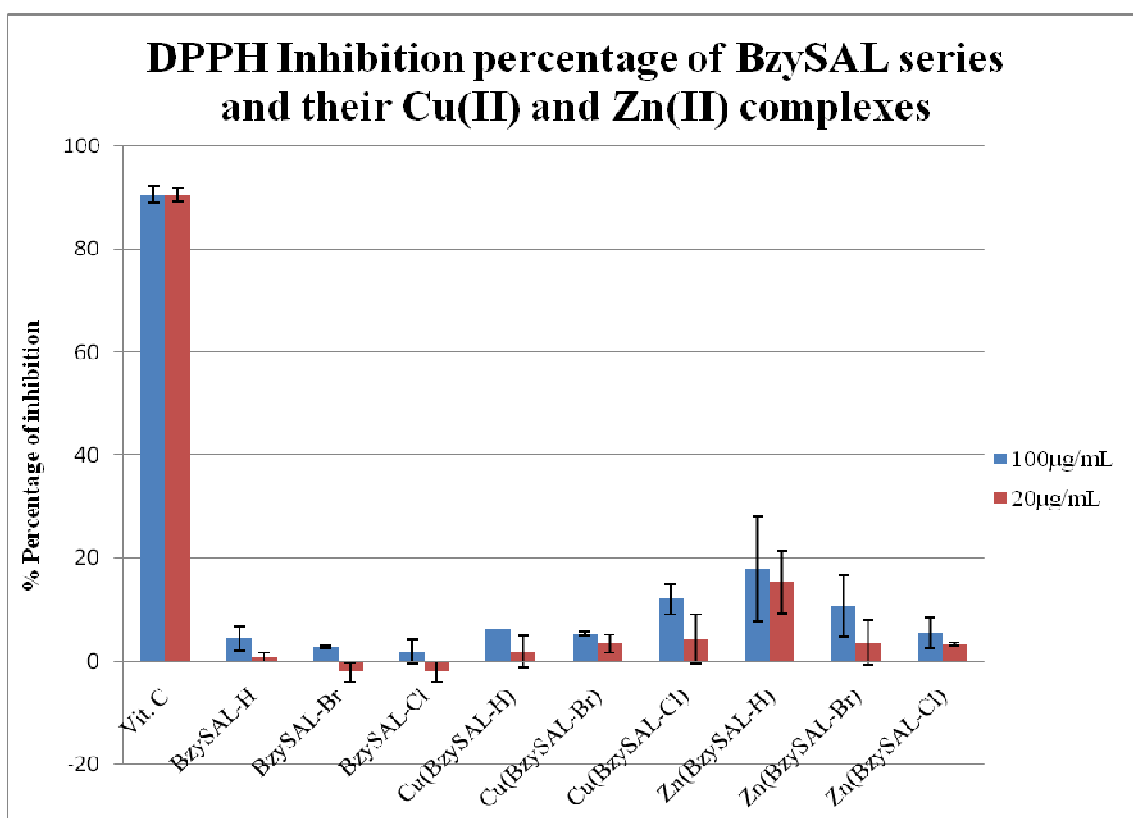


Figure 4.43: DPPH inhibition percentage of BzySAL series and their Cu(II) and Zn(II) complexes

4.4.4 FRAP Value of Ligands and complexes of BzyHAP series

The ferric reducing anti-oxidant power (FRAP) of the compound measured in comparison with vitamin C as the standard. The results obtained are expressed in μM ferrous equivalents and are tabulated in the bar chart (Figure 4.44). From all compounds in the series, only $\text{Zn}(\text{BzySAL-H})$ is recorded having slightly higher FRAP value than the standard. Nevertheless, the reduction of the tested ferric TPTZ complex against other compounds in the FRAP assays are lower than vitamin C. The $\text{Cu}(\text{II})$ and $\text{Zn}(\text{II})$ complexes of BzySAL-H show higher FRAP value than the parent ligand. The $\text{Cu}(\text{BzySAL-Br})$ displays higher FRAP value compared to the free ligand and the $\text{Zn}(\text{II})$ complex whereas $\text{Zn}(\text{BzySAL-Cl})$ records the lowest.

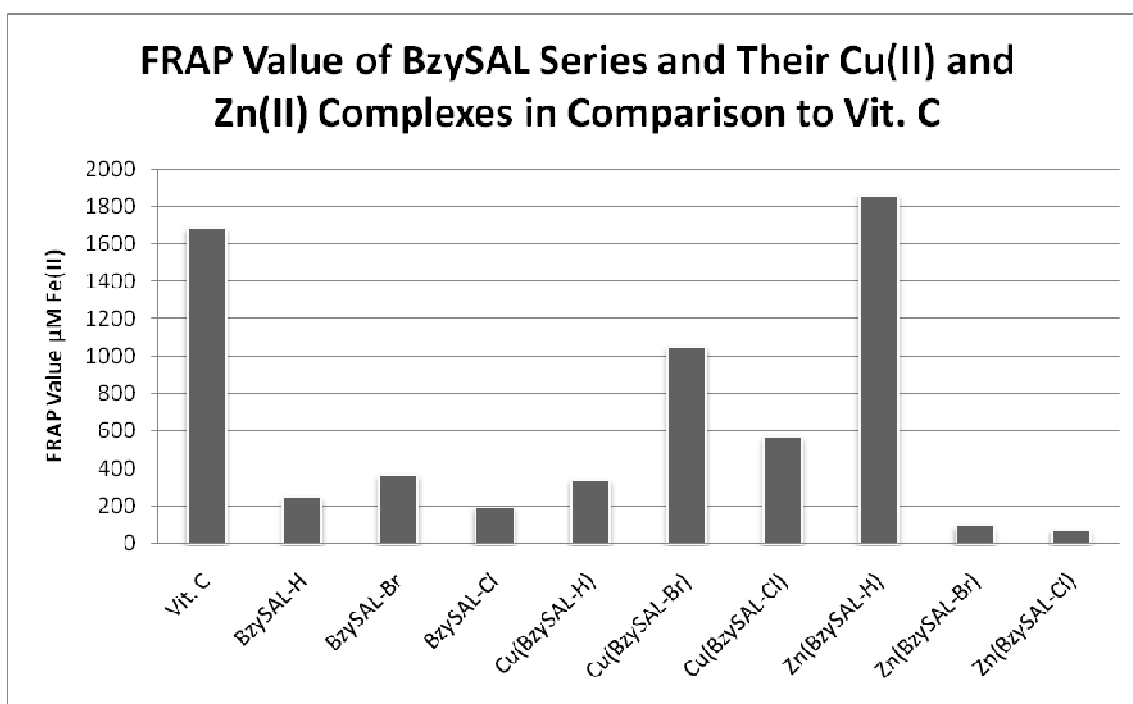


Figure 4.44: FRAP value of BzySAL series and their $\text{Cu}(\text{II})$ and $\text{Zn}(\text{II})$ complexes

CONCLUSIONS

In this study, all desired Schiff base ligands and complexes were successfully synthesized. From the IR spectra, the formation of the ligands is confirmed by the exhibition of new imine band resided around the region of 1590-1619 cm^{-1} . The ^1H NMR and ^{13}C NMR analyses demonstrate that all protons and carbons are found at their expected region and in a good agreement with the proposed structures.

The coordination of the ligand to Cu(II) and Zn(II) ion is confirmed by the shift of $\nu(\text{C}=\text{N})$ band and the exhibition of new $\nu(\text{M}-\text{O})$ and $\nu(\text{M}-\text{N})$ band. The absence of $\delta(\text{N}-\text{H})$ and $\delta(\text{O}-\text{H})$ of the hydroxyacetophenone and salicylaldehyde moiety in the ^1H NMR spectrum of Zn(II) complexes confirms that the ligand-metal ion coordination occurs via phenolic oxygen, imine nitrogen and carbonyl nitrogen atom (O,N,O). Although the attempt to grow crystal of the complex is unsuccessful, the structures are predicted by the result of UV-Vis and AAS analyses.

The toxicity screening of the compounds reveals that all ligands and their Zn(II) complexes are inactive cell growth inhibitor. Nonetheless, it can be concluded that the coordination of the ligand to Cu(II) ion increases the growth inhibition potential of the ligand.

From the DPPH scavenging capacities evaluation, all compounds show significantly moderate DPPH inhibition compared to the standard vitamin C. The highest DPPH inhibition percentage is recorded by the unsubstituted BzyHAP-H ligand. In addition, none of the compounds reduce the ferric TPTZ complex used in the FRAP assay better than the vitamin C as the standard.